



This is a repository copy of *Methylammonium-free wide-bandgap metal halide perovskites for tandem photovoltaics*.

White Rose Research Online URL for this paper:

<https://eprints.whiterose.ac.uk/212350/>

Version: Accepted Version

Article:

Ramadan, A.J. orcid.org/0000-0003-4572-3459, Oliver, R.D.J. orcid.org/0000-0003-4980-7940, Johnston, M.B. orcid.org/0000-0002-0301-8033 et al. (1 more author) (2023) Methylammonium-free wide-bandgap metal halide perovskites for tandem photovoltaics. *Nature Reviews Materials*, 8 (12). pp. 822-838. ISSN 2058-8437

<https://doi.org/10.1038/s41578-023-00610-9>

This version of the article has been accepted for publication, after peer review (when applicable) and is subject to Springer Nature's AM terms of use, but is not the Version of Record and does not reflect post-acceptance improvements, or any corrections. The Version of Record is available online at: <http://dx.doi.org/10.1038/s41578-023-00610-9>

Reuse

Items deposited in White Rose Research Online are protected by copyright, with all rights reserved unless indicated otherwise. They may be downloaded and/or printed for private study, or other acts as permitted by national copyright laws. The publisher or other rights holders may allow further reproduction and re-use of the full text version. This is indicated by the licence information on the White Rose Research Online record for the item.

Takedown

If you consider content in White Rose Research Online to be in breach of UK law, please notify us by emailing eprints@whiterose.ac.uk including the URL of the record and the reason for the withdrawal request.



eprints@whiterose.ac.uk
<https://eprints.whiterose.ac.uk/>

Methylammonium-free wide bandgap metal halide perovskites for tandem photovoltaics

Alexandra J. Ramadan^{1,2*}, Robert D. J. Oliver^{1,2}, Michael B. Johnston², Henry J. Snaith²

1. Department of Physics and Astronomy, University of Sheffield, Sheffield, UK

2. Department of Physics, University of Oxford, Clarendon Laboratory, Parks Road, Oxford, UK

Corresponding author: a.ramadan@sheffield.ac.uk

Abstract

Over the past decade, the performance of solar cells based on metal halide perovskite (MHP) semiconductors has skyrocketed, now rivalling established technologies such as crystalline silicon. However, the most promising implementation of MHP semiconductors is in a tandem solar cell which promise and have indeed delivered far higher power conversion efficiencies. The tuneable bandgap of MHPs makes them uniquely placed to deliver these high-efficiency tandem solar cells for a range of different narrow bandgap absorbers. Tandem devices based on methylammonium containing wide bandgap (> 1.7 eV) absorber top cells have achieved efficiencies over 30%, an impressive achievement¹. Despite this, tandem devices based on methylammonium-free wide bandgap absorber top cells are yet to reach the 30% efficiency milestone. Methylammonium-free wide bandgap MHPs perform particularly poorly compared to their methylammonium containing and narrower bandgap counterparts, illustrating significant scope for even greater advances in tandem cell technology. In this review, we focus on the methylammonium-free MHPs. We highlight the unique challenges faced by these materials, including the energy-loss pathways that currently constrain their open-circuit voltage and efficiency well below their thermodynamic limits. We discuss recent progress in the development of this material system, their performance in tandem photovoltaics and highlight research trends that seem particularly promising. Finally, we suggest future avenues to explore to expedite the development of wide bandgap MHPs which will in turn accelerate the deployment of tandem solar cells based on these materials.

Introduction

Metal halide perovskite semiconductors have been the subject of intense research effort in the photovoltaic and broader optoelectronics research community over the past decade. This has led to soaring power conversion efficiencies (PCEs) of single junction perovskite solar cells, which now rival those achievable with crystalline silicon.² This is largely a consequence of their excellent optoelectronic properties such as high charge-carrier mobilities^{3–5} long charge-carrier diffusion lengths,^{6,7} high absorption coefficients^{8–10} and low energetic disorder characterised by small Urbach energies.^{11–13} Another key property of metal halide perovskites is their broadly tuneable optoelectronic properties achievable through careful choice of the constituents in the ABX_3 crystal structure. In such a way, a boundless choice of bandgaps between 1.2 – 3.2 eV are achievable.¹⁴ Owing to this property, perovskites can be tailored toward a specific photovoltaic application. One particularly significant application is for use as the top cell in a tandem photovoltaic device (Fig. 1a,b), which requires a bandgap between 1.67 – 1.8 eV.^{15,16} Indeed, it is (widely) believed that

perovskite semiconductors will first make an impact in the global photovoltaic market as the top cell component of tandem technologies, first in conjunction with crystalline silicon and then in perovskite/perovskite tandems.

The rear cells in perovskite-based tandem solar cells perform excellently and are not the main limiting factor for future tandem developments. Crystalline silicon (c-Si) is well-established as a high efficiency photovoltaic technology and copper indium gallium selenide (CIGS) is a well-industrialised technology. For all-perovskite tandem photovoltaic devices, the rear cells, fabricated from alloying Pb and Sn on the B-site, have recently enjoyed an outstanding improvement in their photovoltaic device performance, and are now approaching their thermodynamic limit for open-circuit voltage.^{17,18} Overcoming reproducibility and long-term stability issues for the narrow bandgap Pb-Sn perovskites are key challenges, but are not the subject of this review. The initial power conversion efficiency of wide bandgap perovskite top cells has not experienced the same successes and are therefore currently the subject of significant investigation. Typically, the wider bandgap materials are achieved by incorporating an increasing alloy fraction of bromide to iodide on the X-site of the perovskite semiconductor's crystal structure. Despite recent progress, devices based on wide bandgap perovskite semiconductors are still constrained below their theoretical maximum performance. This is largely a result of the open-circuit voltage (V_{oc}) of such cells not increasing with increasing bandgap as expected. Achieving voltages >1.2 V has proven challenging.¹⁹ This limited performance has been particularly true for the methylammonium-free metal halide perovskites.^{20–23} Excitingly, recent works have reported voltages of ~ 1.3 V for methylammonium-free perovskites with bandgaps of ~ 1.8 eV demonstrating that these challenges are not inherent to these materials.^{24–26}

It is worth noting that alongside their implementation in photovoltaics, wide bandgap metal halide perovskites have proven highly successful as the emissive layer in light emitting diode (LED) devices.^{27–29} Whilst different contact layers and excitation intensities are present within the two technologies, the success of PeLEDs is an excellent indicator of the potential of high-bromide content perovskites for success in photovoltaic applications. Within the perovskite LED community, photoluminescence quantum yield (PLQY) measurements are routinely used to screen perovskite compositions and determine their potential for producing high electroluminescence external quantum efficiency (EL-EQE) LED devices. There have been many reports within the LED literature of PLQY values exceeding 30 % for wide-bandgap perovskite thin-films, and even exceeding 70 % for materials with bandgaps approximately suitable for tandem PV applications.³⁰ However the reported PLQY values for similar perovskites employed in solar cells are typically at least an order of magnitude lower.^{31–34} It is well established that through applying quasi-Fermi level splitting (QFLS) analysis, PLQY measurements can predict the maximum V_{oc} achievable with a specific materials system or device stack.³⁵ As such, there is a direct correlation between higher PLQY and higher achievable V_{oc} values. We therefore believe that the successes of the perovskite LED community in developing perovskite thin-films with impressive PLQY values and LED devices with high EL-EQE efficiencies is an excellent indicator that the voltage losses plaguing the

wide-bandgap PV community are not inherent to the high-Br perovskite materials system. Instead, we posit that these losses are a direct result of the routes and methods through which we fabricate our perovskite materials and the contact layers implemented in solar cell devices.

In this review we provide an overview of the developments within the field of methylammonium-free wide bandgap metal halide perovskite tandem photovoltaics. We highlight the challenges which the field has yet to overcome and comment on the areas which we think require particular attention to allow the realisation of highly efficient perovskite-based tandem photovoltaics. We discuss the current state of understanding of the fundamental properties of the perovskite material and the influence this exerts over corresponding photovoltaic device performances. This review will focus on materials with bandgaps within the range of 1.6 - 1.9 eV and examine the approaches employed to overcome the challenges in developing and incorporating these wide bandgap perovskite materials in tandem photovoltaics.

Measuring the performance of wide bandgap photovoltaics

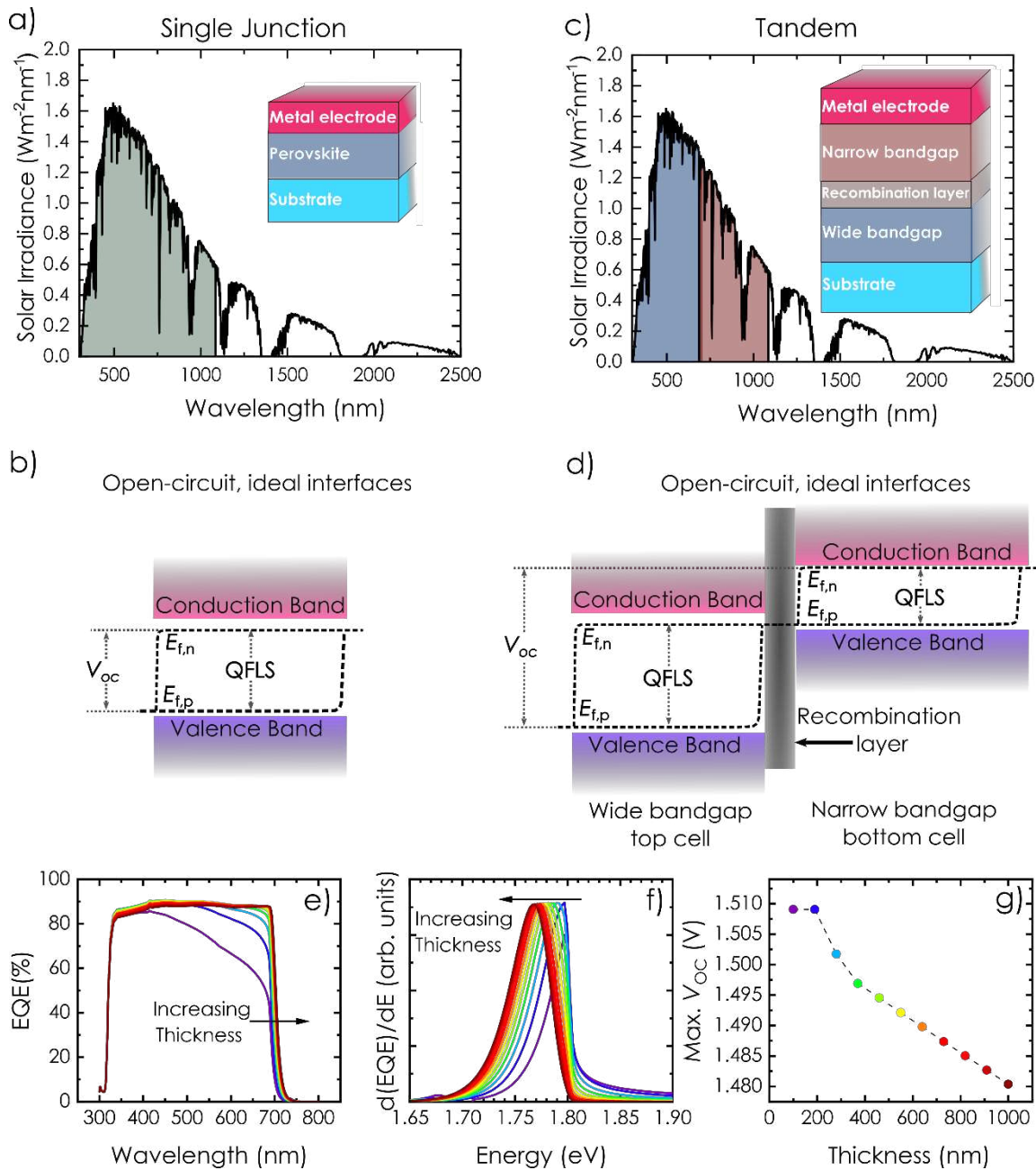


Figure 1 - Tandem device physics. a) The solar irradiance absorbed by a single junction solar cell, shown schematically in the inset, is denoted in green. This leads to a quasi-Fermi level splitting (QFLS) which, assuming perfect contacts, is the V_{oc} measured at the contacts shown in b). c) The solar irradiance absorbed by a tandem solar cell, shown schematically in the inset, is in two contributions. The high energy photons are absorbed by the wide bandgap top cell, denoted in purple, and the lower energy photons are absorbed by narrow bandgap bottom cell, denoted in pink. This results in a QFLS in each sub-cell which, assuming perfect contacts and recombination layer, sums to provide a larger V_{oc} measured at the contacts than is possible with a single junction cell which we show in panel d). e) Simulated external quantum efficiency (EQE) of a wide bandgap perovskite with a range of thicknesses. The intrinsic (electronic) bandgap was held constant at 1.8 eV while the thickness of the perovskite was varied across a range of 100 – 1000 nm with steps of 90 nm. As the thickness increases, the EQE onset is redshifted. f) $d(EQE)/dE$ corresponding to the EQE in panel e). The peak of $d(EQE)/dE$ is shifted to lower energies as the thickness is increased,

which reduced the maximum attainable V_{oc} as summarised in g). A reduction of ~ 30 mV in the maximum attainable open-circuit voltage is possible from simply tuning the perovskite thickness.

For most of the development of perovskite photovoltaics, the solar-to-electrical power conversion efficiency (PCE) was the key figure of merit used in the field. However, as the field moves towards the development of wide bandgap semiconductors for multi-junction applications, comparing PCEs is no longer a useful metric as wide bandgap sub-cells are fundamentally able to harvest less of the available solar spectrum, constraining their maximum feasible PCE. Instead, it is important to reference the performance to the thermodynamic limit at that bandgap. There exists a multitude of methods in the field to determine the bandgap of the perovskite semiconductor. Regrettably, each of these methods can yield a different bandgap for the same material which makes comparison of materials properties of PV device performance difficult across the literature. Further discussion pertaining to bandgap determination can be found in work by Krückemeier and co-workers.³⁶

It is imperative that a consistent method is employed to determine the bandgap of the perovskite semiconductor, especially when integrated in a complete PV device. In most cases, the most useful information brought by the bandgap is the maximum achievable PCE for that PV device incorporating a specific absorber material, which should be the closest approximation to a step-function bandgap, often employed in detailed balance limit calculations. We call this the photovoltaic bandgap, E_g^{PV} , for the PV cell incorporating the given solar absorber material. As highlighted by Nayak and co-workers, this is not an intrinsic material property and will, in many cases, differ from the value of the bandgap determined from optical measurements.³⁷ We highlight this by performing combined optical and drift-diffusion simulations in which we vary the thickness of the perovskite semiconductor, whilst keeping its intrinsic bandgap constant, full details for these simulations can be found in the supplementary information. Fig. 1e shows the shifting of the EQE onset with increasing thickness of the perovskite layer. This correlates to a shift in E_g^{PV} to lower energies (Fig. 1f), which in turn influences the maximum obtainable open-circuit voltage (Fig. 1g) and the device performance. These simulations also show the importance of employing the inflection point in the PV external quantum efficiency to be the method by which E_g^{PV} is determined. This method has numerous advantages which we briefly discuss. Importantly, for a given bandgap determined this way, there is a minor difference in the short circuit current (J_{sc}) for varying sharp absorption onsets. We believe this is a key feature since the bandgap of a solar cell should determine how much of the solar spectrum is available to be harvested. Further, this definition is becoming more widely adopted in both theoretical treatments and in the comparison of different PV technologies.^{37–39} Pragmatically, this method is easy to implement and yields an unambiguous value of the photovoltaic bandgap for materials with a sharp absorption onset like mixed-halide perovskite solar cells. To determine the bandgap this way, one simply needs to find the maximum value of $d(EQE)/dE$, which is easily done numerically. We wish to highlight the work of Almora and co-workers who extend this approach to work for emerging PV materials that may not have a sharp absorption onset, and relate this to recombination behaviour with the device.⁴⁰ See the supplementary information for discussion on bandgap determination for fundamental materials

properties investigations. This is particularly important when reporting record open-circuit voltages where we recommend following the procedure described by Krückemeier and co-workers.³⁶ Brief details on this are provided in the supplementary information.

Origin of voltage losses in wide bandgap perovskites

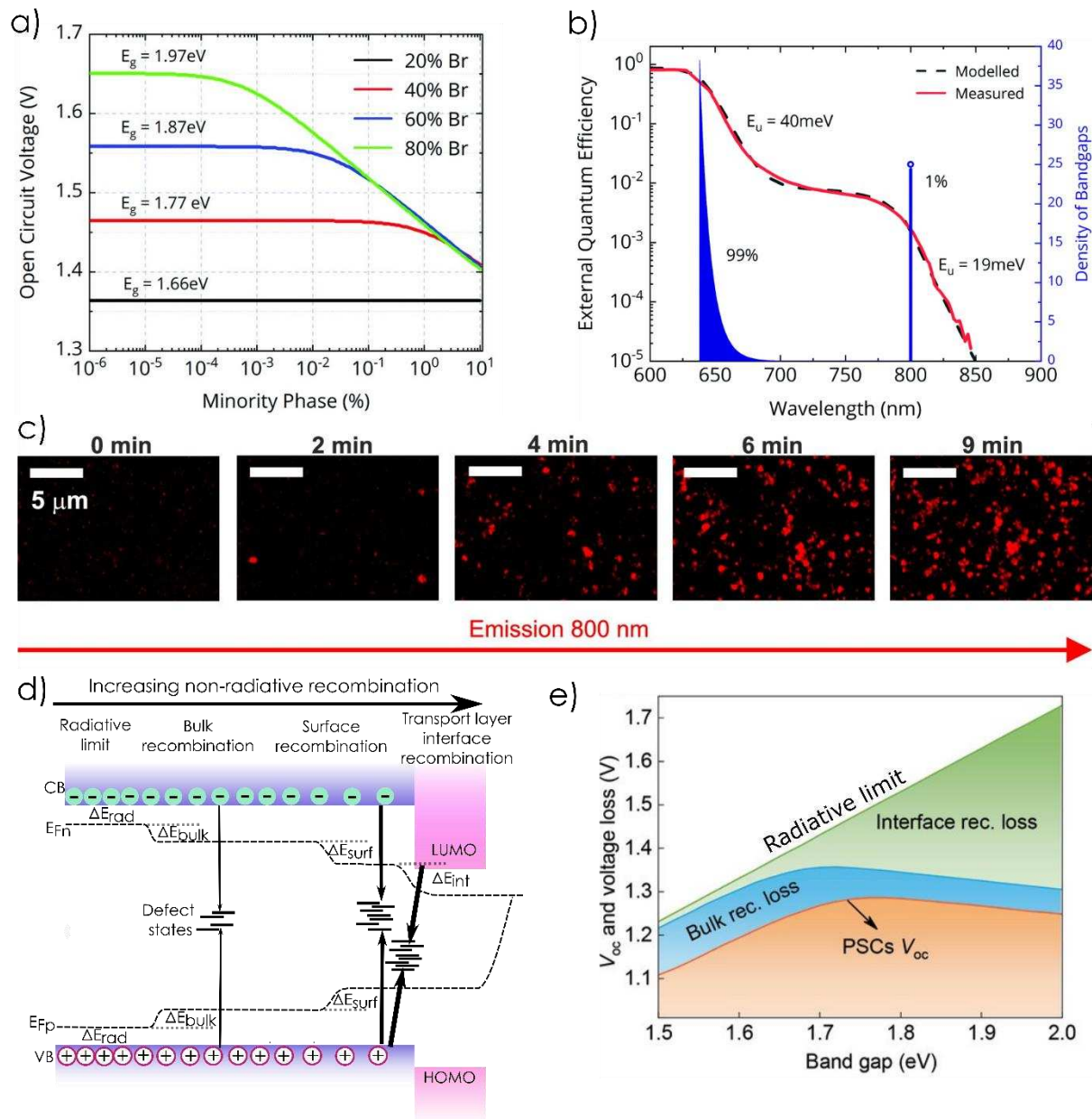


Figure 2 - Halide segregation and voltage losses. a) Effect of halide segregation on the photovoltaic external quantum efficiency (EQE_{PV}) shown in solid red. The dashed line is the modelled EQE_{PV} assuming the distribution of bandgaps in the perovskite solar cell shown in blue. Only $\sim 1\%$ of the film is in the minority (segregated) phase. b) Radiative limit open-circuit voltage as a function of the percentage of the minority phase (assumed to be 20% Br). For higher the initial bandgaps (Br content), the perovskite solar cells can accommodate a smaller fraction of segregated phase before a dramatic reduction in the open-circuit voltage. c) Different time frames of 800 nm (segregated phase) emission from cathodoluminescence measurements indicating the small domain size for the segregated phase. d) Schematic demonstrating the effect of non-radiative recombination

within the bulk, at the perovskite surface and at the interface with charge transport layers. For simplicity, we have assumed that defects are equally likely to trap electrons and holes. e) The relative contribution of bulk and interfacial losses (including both surface & transport layer interface traps) as a function of bandgap. Panels a-b adapted from ref.⁴¹ Panel c adapted from ref.⁴² Panel e adapted from ref.⁴³

A key challenge in the development of photovoltaics based on wide bandgap metal halide perovskites is the difference between the theoretically achievable voltages and those which have been experimentally achieved. Increasing the bromide-to-iodide ratio on the X-site in the perovskite crystal structure, results in a widening of the perovskite bandgap. However, the open-circuit voltage of PV devices does not follow a similar trend and in perovskite compositions with $\geq 20\%$ Br inclusion achieving an open-circuit voltage beyond ~ 1.2 V has proven challenging.¹⁹ Recent reports have emerged reporting open-circuit voltages of 1.3 V and beyond for wide bandgap perovskites with bandgaps of ~ 1.8 eV.^{24–26} These reports, and the approaches utilised to achieve these impressive voltages will be discussed in more detail later. In high-Br systems the phenomenon of halide segregation is observed. This is a process in which the different halide species physically separate in the perovskite material, usually driven by above bandgap illumination or current injection. The separation of different halide species leads to a heterogeneous energy landscape within the perovskite semiconductor which has numerous implications for both the fundamental physics and device applications of wide bandgap perovskites. For an in-depth review of halide segregation and its influence on material properties we recommend the perspective from Knight and Herz⁴⁴, herein we instead briefly discuss on the implications of halide segregation on device performance.

At Br fractions of $\sim 20\%$ and higher, halide segregation becomes prevalent under illumination which results in the formation of iodide-rich regions which possess lower-than-desired bandgaps. Therefore, charges in the well-mixed wide bandgap phase funnel into these regions, losing energy in the process and hence reduce the achievable V_{oc} of high Br-content perovskites. This funnelling results in high charge carrier densities in the I-rich phase, which in turn leads to extremely prevalent low energy photoluminescence.^{45–47} However, the degree to which this process affected device performance was not fully understood until recently.

Mahesh and co-workers quantified the extent to which halide segregation affects the open-circuit voltage in state-of-the-art metal halide perovskite solar cells.⁴¹ In this study, the band-edge of full photovoltaic devices was characterised using high sensitivity Fourier-transform photocurrent spectroscopy to determine the external quantum efficiency of devices before and after halide segregation (Fig. 2a). Detailed-balance calculations were then applied to fully quantify the effects of halide segregation on PV device performance. In this way, Mahesh and co-workers unambiguously determined the V_{oc} penalty associated with halide segregation (Fig. 2b), discovering that halide segregation could only account for a small fraction of the lost voltage, and there were more significant losses elsewhere in the device architecture. This observation is true for

the most commonly employed perovskite A-site compositions (e.g. FACs, FAMA, and FAMACs), and so demonstrates that careful optimisation of the device architecture of wide-bandgap perovskite solar cells is of the utmost performance to unlock their full potential. Explicitly, halide segregation could account for an additional V_{oc} loss of ~ 100 mV. By reconciling the detailed-balance calculations with experimental observations, some remarkable properties about the halide segregation process and its influence on device performance were revealed. Firstly, only a small volume of the film, $\sim 1\%$, needs to have undergone halide segregation to have a significant impact on the device's V_{oc} . In addition, quantitative evidence was provided that the segregated minority phase suffers from less non-radiative recombination than the majority, well-mixed phase, through a 19-fold enhanced electroluminescence quantum efficiency. These conclusions were confirmed by the work of Caprioglio and co-workers through the observation of small, halide segregated domains in cathodoluminescence measurements on a range of $FA_{1-x}Cs_xPb(Br_yI_{1-y})_3$ thin films (Fig. 2c).⁴² Using photoluminescence spectroscopy measurements it was shown that these small, halide segregated domains possessed high PLQYs, higher than that which is achievable through deliberate synthesis of these compositions. These observations are not simply limited to $FA_{1-x}Cs_xPb(Br_yI_{1-y})_3$ perovskites and agree strongly with the observations made by Peña-Camargo and co-workers on the triple-cation FAMACs perovskite.⁴⁸ Interestingly, work by Motti and co-workers suggests that, despite being funnelled into the narrower bandgap regions, charge-carriers are not trapped in the iodide-rich domains.⁴⁷ This conclusion arises from observation that the charge-carrier mobility within the iodide rich domain is unchanged compared to the well-mixed wide bandgap phase. This is the case for MA- and FACs-based perovskite semiconductors. It should be noted that in systems that undergo halide segregation, extreme care needs to be taken if QFLS analysis is to be performed. This is because, in phase-segregated materials the absorption and emission are from different materials, the well-mixed wide bandgap and the iodide-rich narrow bandgap domains respectively. This violates the principle of optical reciprocity, on which the QFLS depends.

In brief, halide segregation often results in an enhancement in the photoluminescence yield, which crucially does not correspond to an enhancement to the open-circuit voltage of a PV device based on this material. Recent works have shown a strong correlation between the heterogeneity of the perovskite absorber and the degree to which it undergoes light induced halide segregation.⁴⁹ Reducing heterogeneity enables higher open circuit voltages, in part due to a reduction in defect activity.⁴⁵ For an excellent review into defect activity within MHP semiconductors, we recommend the work of Zhou and co-workers.⁵⁰ Here, we summarise the important details regarding wide bandgap MA-free perovskites. In Fig. 2d, we show how different recombination pathways affect the QFLS and in turn the maximum achievable open-circuit voltage. Due to the principle of detailed balance, there will always radiative recombination occurring within the PV device which results in an unavoidable loss in potential energy, which we denote here as ΔE_{rad} . Any further loss from this so-called radiative limit (i.e. wherein all recombination is via these unavoidable radiative channels) occurs through non-radiative recombination pathways. At charge-carrier densities typical in wide bandgap devices under 1 sun illumination, Auger recombination is negligible and so we do not discuss it further. Therefore, the remaining non-radiative losses occur by recombination via a trap

state which occurs within the bulk of the material, at the surface and interfaces with charge transport layers. Our simplified diagram in Fig 2d assumes that these traps are equally likely to trap electrons and holes. Trap-mediated recombination within the bulk of wide bandgap materials is typically much more significant as compared to their lower bandgap counterparts,⁵¹ resulting in a loss of potential energy we denote as ΔE_{bulk} . Density functional theory predicts that halide interstitials are among the most thermodynamically stable which can introduce deep trap states.⁵² It is suggested that short-lived hole traps becomes increasingly prominent as the Br-content is increased within the MHP semiconductor which could explain the relatively low PLQYs in these materials.⁵⁰ The next most significant recombination pathway within these materials is at the surface and grain boundaries of the MHP material, reducing the potential energy further by ΔE_{surf} and typically $\Delta E_{\text{surf}} \gg \Delta E_{\text{bulk}}$. This surface-recombination is typically much more substantial within high Br materials. The organic bromide species (e.g FAPbBr) is more volatile than the iodide-based equivalent, which can leave high-Br MHP semiconductors relatively more AX deficient on the surfaces resulting in increased PbX₂-termination.⁵³ This type of surface termination can lead to increased I₂ and metallic lead formation on the surface which reduces the performance and stability of these materials.⁵⁴⁻⁵⁷ It is our belief that passivating these surface and bulk defects will also reduce the degree of halide segregation by increasing the barrier to ionic rearrangement. Finally, there is a further potential energy loss, ΔE_{int} , associated with recombination at, or across, the perovskite / charge transport layer interface. Poor energetic alignment between the MHP semiconductor and adjoining transport layer also increases the severity of these ΔE_{int} losses. The relative importance of interface over bulk losses is summarised in Fig 2e as a function of the MHP bandgap.

Recently we determined that voltage losses observed in FA_{1-x}CS_xPb(Br_yI_{1-y})₃ perovskite photovoltaics are the result of non-radiative recombination occurring at the perovskite/charge transport layer interfaces.⁵¹ Ultraviolet photoemission spectroscopy and PLQY measurements demonstrated that in our device architecture there was a significant energy level alignment mismatch between the perovskite and the hole transporting layer which resulted in significant non-radiative recombination. Implementation of a passivation strategy at this interface helped to mitigate these losses, and boost device performance, demonstrating the clear gains to be made in V_{oc} by optimising the energetic alignment this interface.

These observations indicate that a thorough understanding of the non-radiative loss mechanisms within wide bandgap perovskites is necessary, and an efficient mitigation strategy must be developed to unlock the potential of these materials for the eventual realisation of highly efficient tandem solar cells. Since 2016 incredible developments have been made in this area. Figure S1 shows reported device parameters for tandem devices with methylammonium-free wide bandgap top cells. Across all tandem architectures, clear gains can be seen in reported V_{oc} . An overview of approaches which can be used to analyse V_{oc} losses in perovskite semiconductors is provided in Supplementary Note 3. In this review, we summarise the developments made in the field to reduce these losses and suggest fruitful avenues for the field to explore.

Challenges of tandem photovoltaic development and fabrication

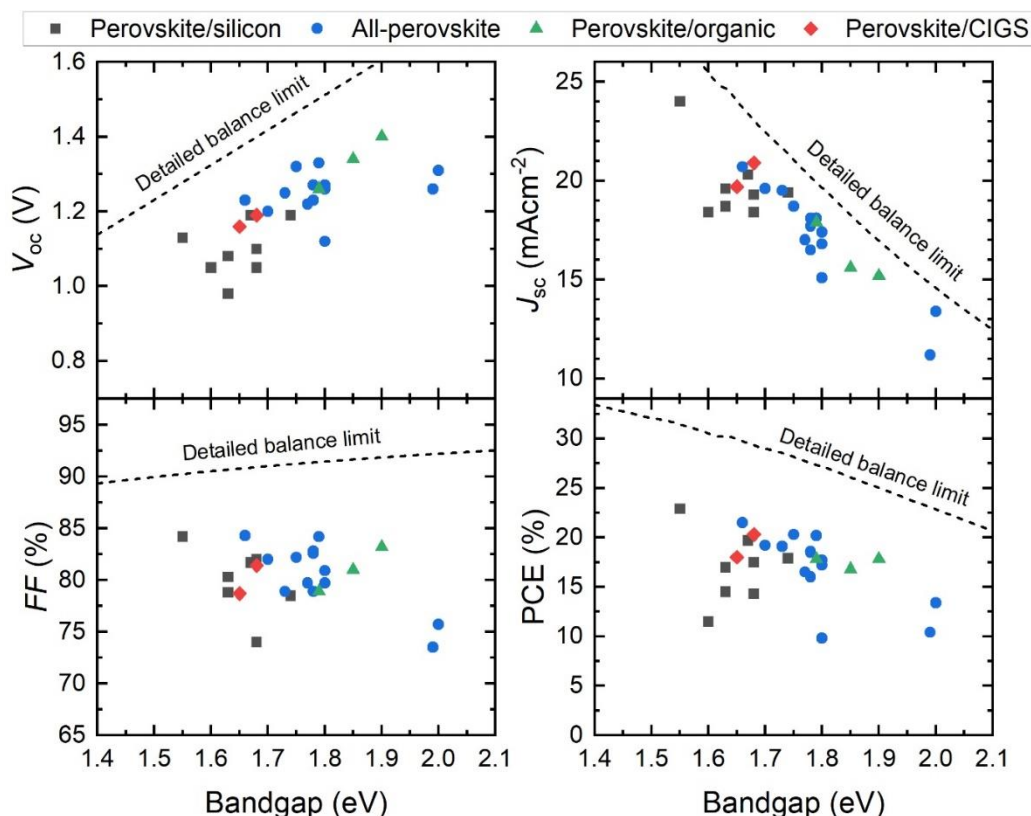


Figure 3: Single-junction performance for MA-free perovskite solar cells as a function of their bandgap. The dashed line indicates the detailed balance limit for each device parameter. Only devices reported in publications that incorporated them into tandems are included. It is evident that there is huge scope for improvements for the MA-free materials with bandgaps approaching 2.0 eV which a required for triple-junction applications.

Tandem photovoltaic devices are typically fabricated as either a two-terminal (2-T) or four-terminal (4-T) structure, with each having their own benefits. In a 4-T tandem, the wide bandgap and narrow bandgap cells are mechanically (and optically) stacked, but electronically contacted separately. This eliminates the current-matching requirements and are in principle easier to fabricate.^{58–60} The 4-T tandem architecture is also more accessible for research labs not set up for the fabrication and characterisation of 2-T tandems, which in principle should allow more research groups to contribute in this area. For optimum energy yield, a 4-T tandem requires two separate junction boxes and electronic interconnects in addition to the use of microinverters, which makes their implementation commercially unproven and hence costly since not yet produced at scale. 4-T tandems could be interconnected to voltage match the top and bottom sub-modules, with overall external power from the module being delivered from two-terminals in the standard fashion. However, this would lower the performance as compared to a monolithic tandem structure due to the unavoidable additional parasitic absorption losses within the internal transparent conductive layers. In contrast, 2-T tandems can provide greater power output for no additional balance of systems costs. Therefore, we recommend the field dedicate its attention to the development and understanding of 2-T tandem

devices where possible. We believe that is for these reasons, despite the additional fabrication challenges, that the field had predominantly focused on the development and understanding of 2-T tandem devices.

The significant challenges in the development of 2-T perovskite-tandems are the development of an ideal perovskite composition that current matches with the bottom cell and the development of the recombination layer. The recombination layer electronically couples the wide and narrow bandgap sub-cells in a tandem device and has stringent requirements for efficient tandem operation. This layer must be deposited in such a way that it does not damage the underlying cell, there are minimal optical losses due to this layer, and it forms an Ohmic contact between the two cells, with low in-plane conductivity.^{15,61} For all-perovskite and perovskite-organic tandems this layer also needs to provide chemical protection during the rear-cell deposition. These challenges are relevant to all types of perovskite tandem devices: all-perovskite, perovskite-on-Si and perovskite-organic and perovskite-CIGS. For a comprehensive review on the challenges and merits associated with the different bottom cells we recommend the work of Ho-Baille and co-workers.⁶²

There are challenges associated with the fabrication and characterisation of perovskite tandem devices, many of which require expensive infrastructure, which have presented significant barriers to the development of perovskite tandem devices. For perovskite-on-Si tandem devices, processing on textured silicon was for a long time incredibly challenging. A significant development in this area was the demonstration that a two-step deposition process (evaporation of the metal halide components followed by a spin-coating of the organohalide components) could result in conformal coverage on textured silicon.⁶³ This approach has been successfully used in the development of methylammonium containing wide bandgap top cells in perovskite-on-Si tandem devices.⁶⁴ Since then there have been a string of additional significant advances in perovskite-on-Si tandem development which have addressed improving the optical properties of the interlayer between the top and bottom junctions, improving the open-circuit voltage of the top perovskite cell via passivation and improved choice of charge extraction layers.⁶⁵⁻⁶⁷

In the case of all-perovskite tandem devices the development of the narrow bandgap absorbing rear cells was a significant challenge in the quest to produce high efficiency all-perovskite tandem devices.⁶⁸ This was in part a consequence of the slow development of tin-based perovskite materials, in comparison to their Pb-based counterparts. The ideal bandgap range for this cell is between 0.9 - 1.3 eV necessitating the use of Sn based perovskite absorber layers. The demonstration of “bandgap bowing” for mixed metal lead-tin perovskites reported by Kanatzidis and co-workers, resulted in the first demonstrations of 2-T and 4-T all-perovskite tandem devices using a Pb-Sn absorber for the rear (narrow bandgap) cell.⁶⁹⁻⁷¹ Consequently, significant developments have been made in reported efficiencies with a large focus of these works being development and optimisation of the Pb-Sn absorber.^{7,72} Whilst reproducibility can be a challenge when fabricating any perovskite photovoltaic device, it is a significant challenge for 2-T all-perovskite tandem devices. Developing perovskite absorbers, processes and tandem architectures which result in high yields is critical to the continued development of these tandem devices. For a

good overview of this problem, and others associated with all-perovskite tandem development we recommend the review by Moot and co-workers.⁷³

Despite, or possibly as a consequence of, organic PV cells having been shadowed by the meteoric efficiency gains of perovskites, there has also been tremendous progress with organic PV cells over the last decade. Specifically with the advent of narrow bandgap non-fullerene acceptors, organic PV cells are now approaching 20 % efficiency in single junctions, with optical bandgaps pushing out into the near IR.^{74–76} This makes them well suited to be coupled with wide bandgap perovskites in monolithic tandem devices. Conveniently, organic semiconductors can often be solution processed using solvents which are orthogonal to those typically used in perovskite photovoltaic deposition, increasing the potential for all solution processed tandem devices.⁷⁷ Recently there have been reports of impressive perovskite-organic tandem devices employing $\text{FA}_{1-x}\text{Cs}_x\text{Pb}(\text{Br}_y\text{I}_{1-y})_3$ compositions for the wide bandgap perovskite top cell which we discuss in more detail later.^{78,79}

Overwhelmingly the field has focussed on double junction architectures, comprised of one narrow and one wide bandgap perovskite cell, but reports of triple junction devices have been made.^{49,80–82} If successful, additional cells enable a broader range of the solar spectrum to be captured, and therefore greater power conversion efficiencies, but additional cells represent significant engineering challenges both in terms of device manufacturing and from an optical management perspective. As development in these areas continues, we expect significant gains will be made in the multi-junction perovskite space. Supplementary Table 1 summarises the performance and stability testing, if available, undertaken for devices discussed throughout this review.

Compositional engineering of the wide bandgap perovskite absorber

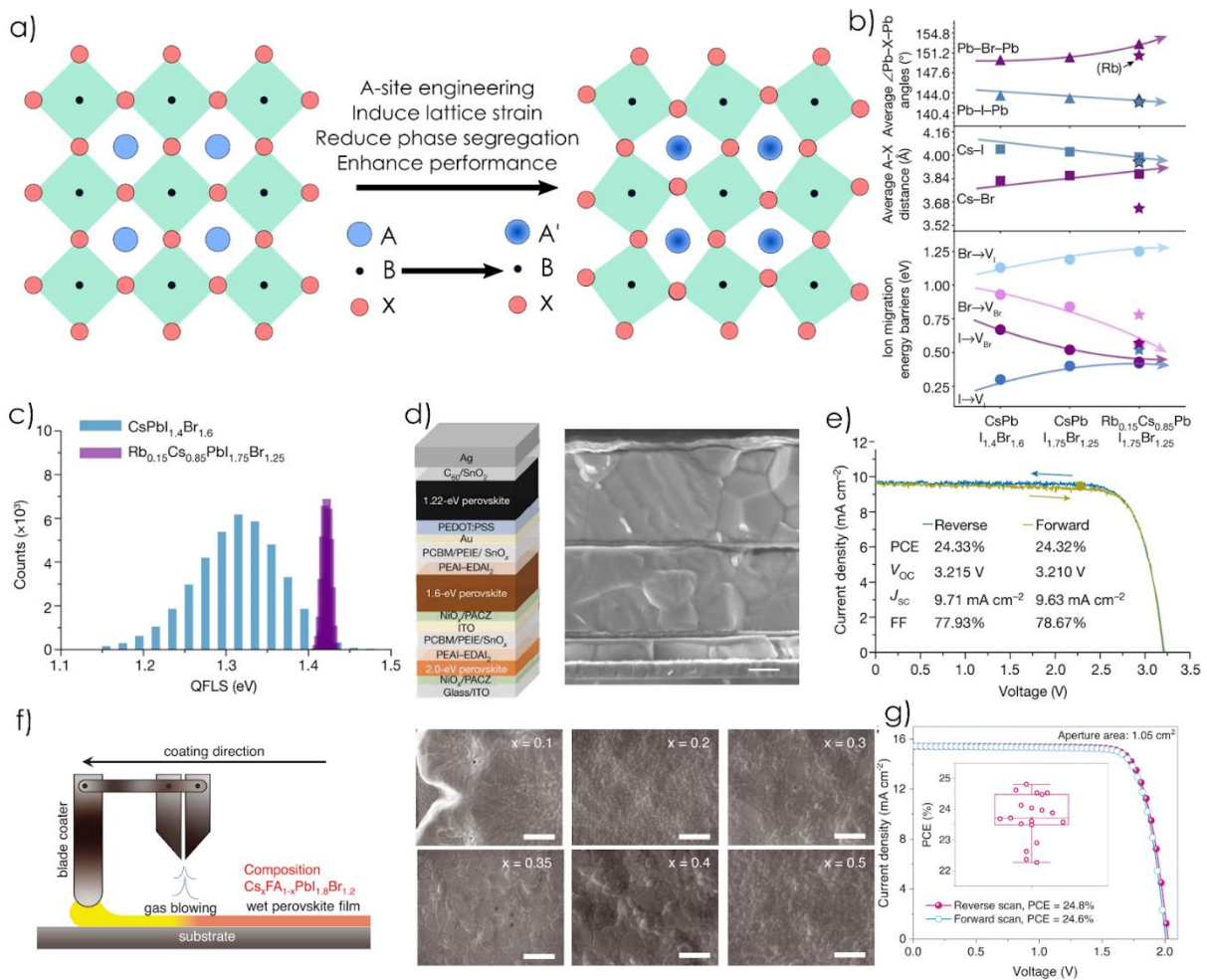


Figure 4 - Compositional Engineering. a) Schematic showing that engineering the A-site composition can lead to octahedral tilting. This changes the orbital overlap and can lead to reduced photoinduced phase segregation and enhanced performance of WBG perovskite solar cells. b) DFT-calculated average Pb-halide-Pb angle, the average A-site cation to halide interatomic distance, and ion migration energetic barrier of I (or Br) to V_I (or V_{Br}) for CsPbI_{1.4}Br_{1.6}, CsPbI_{1.75}Br_{1.25}, and Rb_{0.15}Cs_{0.85}PbI_{1.75}Br_{1.25}. The arrows represent their trends. For Rb_{0.15}Cs_{0.85}PbI_{1.75}Br_{1.25}, the information around the Rb atoms is labelled with stars. c) Histogram of quasi-Fermi level splitting values at each pixel in a hyperspectral image of CsPbI_{1.4}Br_{1.6}, and Rb_{0.15}Cs_{0.85}PbI_{1.75}Br_{1.25} perovskites. The image was 100 μm x 100 μm. The Rb-based perovskite has a significantly tighter distribution of QFLS at higher values, indicative of less phase segregation and higher material quality. d) Schematic of the triple-junction all-perovskite solar cell architecture and corresponding cross-sectional SEM. The scale bar is 400 nm. e) J-V characteristics of the champion triple junction device. f) Schematic of the gas-assisted blade coating technique used to fabricate perovskite thin films with varying cesium-formamidinium-ratios, *x*. SEM micrographs of the different morphologies of the Cs_{*x*}FA_{1-*x*}Pb(I_{0.6}Br_{0.4})₃ thin films, with a scale bar of 1 μm. g) J-V curves of the champion tandem solar cell, active area of 1.05 cm². The inset shows the PCE distribution of 19 devices, where the boxes and whiskers represent the standard deviation and the maximum and minimum of the distributions, respectively. Panels b-e adapted from ref.⁴⁹ Panels f-g adapted from ref.⁸³

Compositional engineering (Fig. 4a) is a well-established route for optimising perovskite photovoltaic device performance. It has proven particularly important in the development of methylammonium-free wide bandgap perovskites as it has been necessary to develop perovskite compositions which have minimal halide segregation to optimise device performance. This is particularly true for compositions suitable for all-perovskite tandems where the required bandgap (~1.8 eV) is wider than that required for perovskite-on-silicon tandems (~1.67 eV). Compositional engineering can be directly controlled by the deposition method through which the perovskite layer is prepared. For a comprehensive overview of the range of deposition methods, their respective benefits, and the influence they can have on photovoltaic performance, we recommend the work of Vaynzof.⁸⁴

The first report of a $\text{FA}_{1-x}\text{Cs}_x\text{Pb}(\text{Br}_y\text{I}_{1-y})_3$ perovskite was from McMeekin and co-workers who demonstrated this absorber layer in both single junction devices and perovskite-on-Si tandems.⁸⁵ Since this initial report it has been demonstrated that there are a wide range of $\text{FA}_{1-x}\text{Cs}_x\text{Pb}(\text{Br}_y\text{I}_{1-y})_3$ compositions which result in similar bandgap materials. In addition to tuning the bandgap and therefore influencing device performance the composition of a perovskite has been shown to influence its stability in a photovoltaic device.^{53,86-89} Bush and co-workers demonstrated the impact of adapting the FA to Cs and I to Br ratios on the bandgap, solar cell performance, and photostability of a range of $\text{FA}_{1-x}\text{Cs}_x\text{Pb}(\text{Br}_y\text{I}_{1-y})_3$ materials.⁹⁰ Subsequently they demonstrated that compositional engineering of the perovskite absorber could improve current matching in 2-T perovskite-on-Si tandem devices based on a $\text{FA}_{0.75}\text{Cs}_{0.25}\text{Pb}(\text{I}_{0.8}\text{Br}_{0.2})_3$ perovskite ($E_g = 1.68$ eV).⁹¹ Their work demonstrated the type of holistic approach required to drive forward the efficiencies of perovskite tandem photovoltaics. Alongside optimisation of the perovskite absorber composition, Bush and co-workers incorporated an alternative charge transport layer and optimised the optical properties of the device by developing the top contact and scattering layer to promote optical absorption in the device and minimise reflection losses.

The introduction of a different charge transport layer can often result in improved device performances, however sometimes this can lead to a need to adapt the composition of the perovskite absorber. One example is the use of nickel oxide (NiO_x). Whilst NiO_x is an attractive *p*-type charge transport layer owing to its impressive stability, its implementation can result in undesirable chemical reactions at the interface with a perovskite absorber layer. To counteract this and produce efficient perovskite-on-silicon tandem devices, Li and co-workers engineered a $\text{Cs}_{0.22}\text{FA}_{0.78}\text{Pb}(\text{I}_{0.85}\text{Br}_{0.15})_3$ perovskite combined with 3 mol% of CsPbCl_3 to simultaneously inhibit reactions with NiO_x and widen the perovskite bandgap from 1.64 eV to 1.67 eV.⁹² With their perovskite absorber, the authors fabricated 2-T perovskite-on-Si tandems (with both *n-i-p* and *p-i-n* architecture) and in the *p-i-n* architecture achieved a champion steady-state PCE = 27.2% and $V_{OC} = 1.86$ V for a device area of 0.5036 cm². Under constant illumination in air (at 25 °C and 20 % relative humidity) the unencapsulated devices were reported to lose 2 % of their initial efficiency after 300 hours.

The interaction of solvent molecules with perovskite precursors, and the chemistry which can occur within perovskite precursor solutions has also been demonstrated to impact the chemistry and physics of perovskite thin films and their corresponding devices. Dimethylformamide (DMF), one of the most used solvents in the fabrication of $\text{FA}_{1-x}\text{Cs}_x\text{Pb}(\text{Br}_y\text{I}_{1-y})_3$ perovskites, has been demonstrated to undergo hydrolysis in the presence of water to form dimethylamine and formic acid which can result in the formation of dimethylammonium lead halide perovskites.^{93–95} The presence of dimethylamine, whether induced by decomposition of the DMF or a result of introduction of acid into the precursor solution, has been shown to improve the solubility of perovskite precursor salts.^{94,95} This consequently reduces the size and concentration of perovskite colloids in a precursor solution leading to the formation of perovskite thin films with larger domains and a higher degree of crystalline orientation. McMeekin and co-workers demonstrated this explicitly for $\text{FA}_{0.83}\text{Cs}_{0.17}\text{Pb}(\text{Br}_{0.2}\text{I}_{0.8})_3$ using hydrohalic acids to control the formation of perovskite colloids in a perovskite in DMF solution⁹⁶ and later expanded this approach, incorporating 2 % K^+ which had been previously reported to minimise hysteresis,^{97–99} to fabricate $\text{FA}_{0.83}\text{Cs}_{0.17}\text{Pb}(\text{Br}_{0.7}\text{I}_{0.3})_3$ ($E_g = 1.94$ eV) perovskite layers for incorporation in solution processed 2-T all-perovskite tandem and triple junction photovoltaics achieving a champion steady-state PCE = 15.20 % and a $V_{OC} = 2.18$ V for the all-perovskite tandem and a champion steady-state PCE = 6.4 % and $V_{OC} = 2.7$ V for the triple junction.⁷⁷

The dimethylammonium cation has been shown to be incorporated into the perovskite crystal structure on the A-site, and its incorporation into the lattice can result in a widening of the perovskite bandgap.^{100–102} For wide bandgap perovskites this has proven to be a useful approach, allowing the bandgap to be increased without the introduction of additional halide anions which can help to avoid halide segregation. Palmstrom and co-workers developed rigid and flexible all-perovskite tandem devices in part through incorporating DMA into their wide bandgap perovskite absorber. Through this approach they engineered a $\text{FA}_{0.6}\text{Cs}_{0.3}\text{DMA}_{0.1}\text{Pb}(\text{I}_{0.8}\text{Br}_{0.2})_3$ perovskite, with a bandgap of 1.7 eV, and combined this with a new type of interconnection layer based on atomic layer deposited aluminium doped zinc oxide (AZO) combined with indium tin oxide/indium zinc oxide (ITO/IZO). When incorporated into rigid all-perovskite tandem devices they reported a champion PCE = 23.1 % and $V_{OC} = 1.88$ V and in their flexible structure they reported a champion PCE = 21.3 % and a $V_{OC} = 1.82$ V.

Similarly in their work on all-perovskite tandem photovoltaics, Wen and co-workers demonstrated the benefit of alloying dimethylammonium and chloride with $\text{Cs}_{0.4}\text{FA}_{0.6}\text{Pb}(\text{I}_{0.75}\text{Br}_{0.25})_3$ and developed a perovskite absorber with a bandgap of 1.8 eV.⁸⁹ With the resulting perovskite absorber ($\text{DMA}_{0.1}\text{Cs}_{0.4}\text{FA}_{0.5}\text{Pb}(\text{Br}_{0.25}\text{I}_{0.75})_{2.85}\text{Cl}_{0.15}$) they reported a champion all-perovskite tandem achieving a steady-state PCE of 26 % and a $V_{OC} = 2.05$ V.

Simple changes to the perovskite thin film fabrication method can have a significant impact on the composition of perovskite thin films. Jiang and co-workers successfully demonstrated this by employing a gas quenching processing step during the deposition of their wide bandgap perovskite layer in their reporting 2-T all-perovskite tandems.²⁶ For a $\text{Cs}_{0.3}\text{FA}_{0.6}\text{DMA}_{0.1}\text{Pb}(\text{I}_{0.7}\text{Br}_{0.3})_3$

perovskite, bandgap of 1.75 eV, the authors reported a champion all-perovskite tandem achieving a PCE of 27.1 % and a $V_{oc} = 2.20$ V. In their work they compare their gas quenched perovskite to a solvent quenched counterpart and demonstrate that when employed in single junction devices the gas quenched perovskite consistently demonstrates better performance across all parameters. Their work demonstrates clearly that the crystallisation of the perovskite thin film is altered by the gas quenching process to produce larger grains with a higher crystalline quality. They suggest that this improvement in crystallinity reduces defects and suppresses light induced halide segregation.

A recent report, from Wang and co-workers, demonstrates the importance of compositional engineering in overcoming voltage losses (due to halide segregation) in the wide bandgap top cell (2.0 eV) in all-perovskite triple junction devices.⁴⁹ Their work builds on previous reports which had demonstrated a correlation between an increase in lattice distortions within mixed halide perovskite structures and a reduction in halide segregation.^{85,103–105} Wang and co-workers employed density functional theory (DFT) (Fig. 4b.) and photoluminescence spectroscopy (Fig. 4c.) studies to probe the relationship between lattice distortions, ion migration barriers, and halide segregation in a range of Rb-Cs based perovskite compositions. Photoluminescence studies, and QFLS analysis, revealed that the Rb-based perovskite has a significantly tighter distribution of QFLS at higher values, indicative of reduced light-induced halide segregation and a reduction in trap state density. Their in-depth exploration of these properties enabled them to develop efficient 2.0 eV perovskite devices, which they demonstrated in all-perovskite triple junctions (Fig. 4d) achieving a certified steady-state PCE = 23.3 % for a device area of 0.049 cm² (Fig. 4e).

Recently Xiao and co-workers reported a significant development in 2-T large area all-perovskite tandem devices.⁸³ To facilitate scale-up, the authors employed blade coating to process the solution processed layers and also tuned the compositional of the perovskite absorbers and their deposition process. Through an extensive investigation of the structure, morphology, and optoelectronic properties of a range of $Cs_xFA_{1-x}PbI_{1.8}Br_{1.2}$ compositions the authors determined $Cs_{0.35}FA_{0.65}PbI_{1.8}Br_{1.2}$ ($E_g = 1.8$ eV) to be an optimal composition for the blade coating process (Fig. 4f). It is common to use an ultra-thin layer of SnO₂ between the C₆₀ charge transport layer and the top electrode to act as a “buffer layer”. Xiao and co-workers added an additional SnO₂ after the modulization scribing, to act as a formal diffusion barrier and inhibit the degradation of the metallic interconnections and perovskite layers. Concomitantly the authors optimised the composition of the Pb-Sn rear cell and achieved a PCE = 25 % for 1cm² devices and a certified PCE = 21.7 % for a 20 cm² module (Fig. 4g). Notably at time of writing this stands as the world record efficiency for a perovskite module.² These encapsulated modules maintained their PCE after dark storage at 40 % RH for 1778 h. Under ambient conditions with constant illumination (AM 1.5 including the UV component) the encapsulated devices maintained 75 % of their initial PCE after 500 h of MPP tracking however modules without the conformal diffusion barrier degraded to less than 50 % of the initial PCE after 20 h. Heating of these encapsulated devices at 85 °C in N₂ was found to have a similar impact with the devices without the ALD-SnO₂ barrier degrading to 10 % of their initial PCE after 312 h and those with maintaining > 70 % of their initial PCE.

As the reported performances of devices have risen, it has become clear that to minimise the effects of light induced halide segregation (and therefore V_{oc} losses) the bromide content needs to be kept as low as possible (<20% where possible, this is unlikely to be possible for ~ 2.0 eV bandgaps). To still engineer a wide bandgap, one approach which can be employed is to increase the caesium content⁸³ however this introduces difficulties with producing highly crystalline, homogenous perovskite thin films (in part due to issues with the solubility of caesium). From recent reports, it seems highly likely that engineering crystallographically strained perovskite absorbers may allow us to overcome V_{oc} losses associated with light induced halide segregation, whether that is due to specific cation engineering (e.g. the incorporation of Rb or DMA as a co-cation on the A-site in addition to Cs) or through highly controlled thin film growth.^{26,49,89,106}

Interfacial passivation of the wide bandgap perovskite absorber

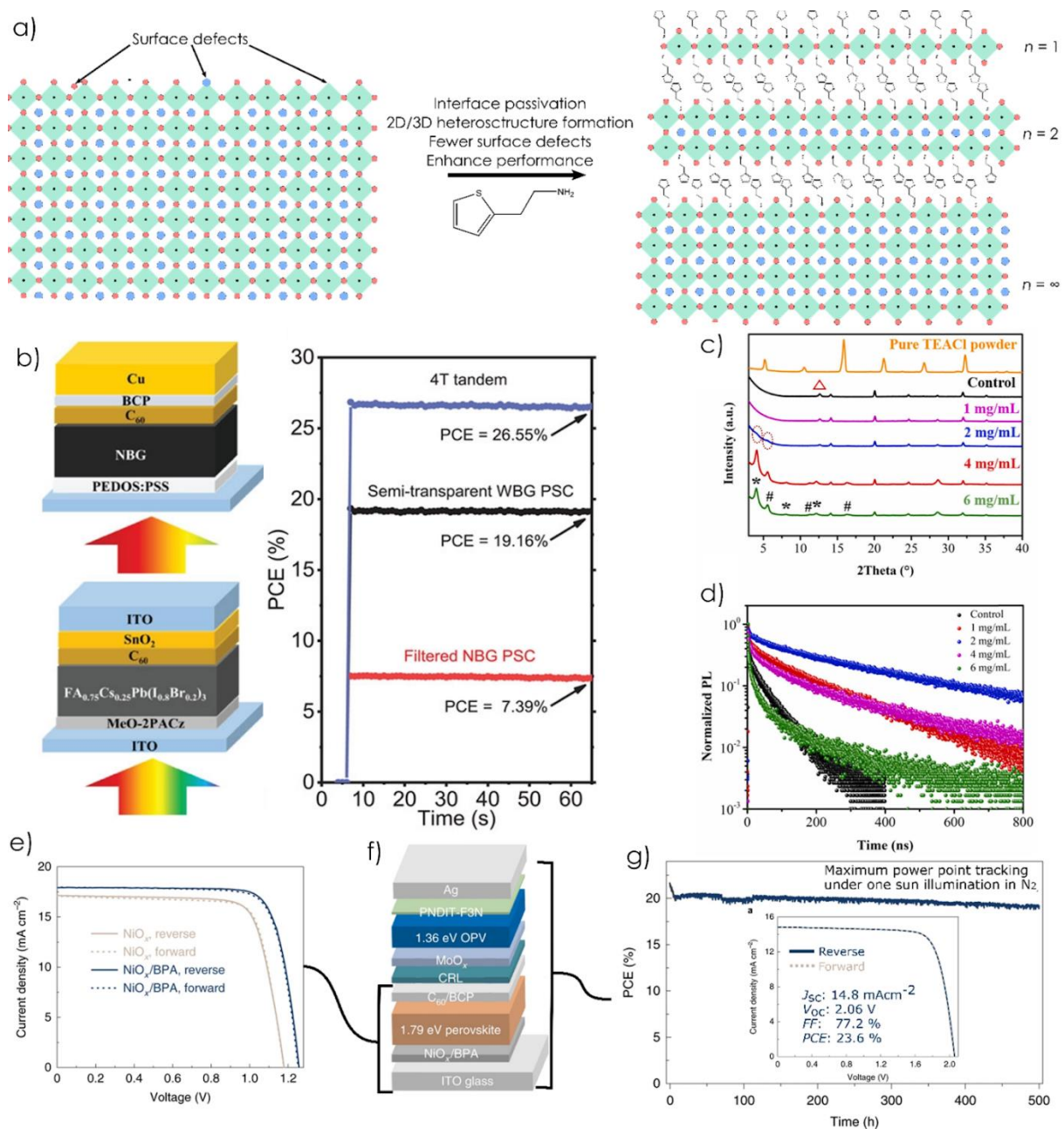


Figure 5 - Interfacial Passivation. a) Schematic illustrating the top passivation technique whereby an additional molecule is applied to the surface of the perovskite after processing. This route can lead to the formation of 2D/3D heterostructures, as shown on the right of the diagram, which can lead to a substantial improvement of device performance. b) Schematic of the 4T tandem which generated the stabilised power outputs shown in the right of the plot. Together, the filtered narrow bandgap and semi-transparent wide bandgap, surface-treated with TEACl, solar cells delivered an SPO of 26.6 %. c) X-ray diffraction patterns of $\text{FA}_{0.8}\text{Cs}_{0.2}\text{Pb}(\text{I}_{0.8}\text{Br}_{0.2})_3$ post-treated with varying concentrations of 2-thiopheneethylammonium chloride (TEACl) in isopropanol. Diffraction peaks assigned to 2D perovskite are visible for concentrations in excess of 2 mg/mL. d) Time-correlated single photon counting measurements of the TEACl-treated samples. The photoluminescence lifetime is increased following TEACl treatment (apart from the highest concentration), indicative of reduced trap-mediated non-radiative recombination. e) J - V characteristics of the champion reference (brown) and bottom passivated with benzylphosphonic acid (blue) solar cells. Treating the NiO_x hole transport layer leads to an enhancement of all device parameters. f) Schematic of the device architecture of the single junction and perovskite-organic tandem devices whose performance is shown in figure e) and g) respectively. g) Maximum power point stability assessment of the perovskite-organic tandem solar cell under one sun illumination in a N_2 -filled glovebox. *Inset:* J - V characteristics of the champion perovskite-organic tandem solar cell. Panel b adapted from ref.¹⁰⁷ Panels c-d adapted from ref.¹⁰⁸ Panels e-g adapted from ref.⁷⁸

Interfacial passivation has been critical to the rapid development of perovskite photovoltaics, and it has proven equally important in methylammonium-free wide bandgap perovskites.^{51,97,109–111} As with perovskites more suitable for single-junction photovoltaics ($E_g \sim 1.55$ eV) and those containing methylammonium, a range of approaches including (but not limited to) ionic additives, ammonium halide salts, thiophene containing molecules and other Lewis bases have been demonstrated to boost the performance of wide bandgap methylammonium free metal halide perovskite photovoltaic devices.^{66,112–121} Whilst not focused on methylammonium-free wide bandgap perovskites, we direct readers interested in additive engineering to the review by Zhang and Zhu for further details.¹²²

In methylammonium-free wide bandgap perovskite tandem devices approaches towards interfacial passivation (Fig. 5a) have predominantly been focussed on improving the interface between the perovskite absorber and the hole transporting layer in n - i - p device architectures. In their development of 4-T perovskite-on-Si tandem photovoltaics, Jaysankar and co-workers implemented an ultra-thin layer of Al_2O_3 (0.8 nm), through ALD, in n - i - p photovoltaic devices based on a $\text{FA}_{0.85}\text{Cs}_{0.15}\text{Pb}(\text{I}_{0.71}\text{Br}_{0.29})_3$ perovskite ($E_g = 1.72$ eV).²² This layer was introduced between the perovskite/spiro-OMeTAD interface in single junction devices and yielded an enhancement in the device's open-circuit voltage, from 1.11 V in the control devices to 1.22 V. This enhancement would be equivalent to an enhancement in radiative efficiency of more than a factor of 70, clearly highlighting just how critical the perovskite/HTL interface is in the n - i - p device structure. This

substantial enhancement of the perovskite device enabled Jaysankar and co-workers to fabricate 4-T perovskite-on-Si tandem devices with a PCE of 27.1 % for a device area of 0.13 cm².

In a similar vein Gharibzadeh and co-workers developed 4-T perovskite-on-Si and on CIGS (copper indium gallium selenide) tandem devices with 2D-3D perovskite heterostructures as a modification at the perovskite/spiro-OMeTAD interface.¹²³ Two-dimensional (2D) perovskite structures such as the Ruddlesden Popper (RP) and Dion Jacobson (DJ) phases can be formed by incorporating bulky monovalent (RP) or divalent cations (DJ) into the A-site of the perovskite structure resulting in the general structures A_{n-1}B_nX_{3n+1} (RP) and A'A_{n-1}B_nX_{3n+1} (Dion Jacobson). The blending of these 2D phases with 3D perovskite to form 2D/3D heterostructures both as an interfacial modification or as a bulk passivation approach have been widely employed as a route to developing perovskite solar cells with long term stability and high efficiency.^{115,124,125} In their work, Gharibzadeh and co-workers used a butylammonium bromide surface post-treatment to form a 2D-3D perovskite heterostructure between a FA_{0.83}CS_{0.17}Pb(I_{1-y}Br_y)₃ perovskite and the spiro-MeOTAD (HTL) interface. This approach was demonstrated for a range of perovskite bandgaps from 1.65 eV – 1.86 eV and a boost in device performance was observed for all reported bandgaps in single junctions. This approach was then demonstrated in tandem devices, using a 1.65 eV perovskite absorber (FA_{0.83}CS_{0.17}Pb(I_{0.76}Br_{0.24})₃) they reported a champion 4-T perovskite-on-Si tandem (Fig. 5b) with a steady-state PCE = 25.7 % and a champion 4-T perovskite-on-CIGS with a steady-state PCE = 25.0 %.

Lewis bases such as thiophene have long been known to act as defect passivants through the propensity of S to bind with undercoordinated Pb²⁺ atoms.¹²⁶ Chen and co-workers exploited this interaction, and built on previous work on methylammonium-containing perovskites¹⁰⁷, to demonstrate quasi-2D thiophene based perovskite heterostructures in devices containing FA_{0.8}CS_{0.2}Pb(I_{0.8}Br_{0.2})₃, ($E_g = 1.68$ eV, Tauc plot) for both single junction (*p-i-n*) and 4-T perovskite-on-CIGS tandem photovoltaic devices.¹⁰⁸ Chen and co-workers employed 2-thiophenethylammonium chloride (TEACl) as a post-treatment for a FA_{0.8}CS_{0.2}Pb(I_{0.8}Br_{0.2})₃ perovskite to form a 2D/3D heterostructure (Fig. 5c) at the perovskite/electron transport layer interface with enhanced charge carrier lifetimes (Fig. 5d). In their tandem devices they reported a PCE of 24 % for the optimal TEACl treated perovskite device. The TEACl treatment was demonstrated to enhance the stability of unencapsulated devices stored in air (~40 % RH) with a retention of 92.8 % of the initial efficiency compared to the control devices which only retained 53.7 % of their initial efficiency. It is unclear if these devices were stored in the dark or light. The treated devices also demonstrated enhanced stability when stored in the dark in N₂ and at 25 and 60 °C.

Interfacial passivation played a key role in the impressive perovskite-organic tandem device performances reported by Chen and co-workers.⁷⁸ In their work the authors utilised NiO_x treated with benzylphosphonic acid as the hole transporting layer in the perovskite top cell and consequently demonstrated a significant suppression in V_{oc} losses (Fig. 5e), reporting an increase of 80 mV relative to their control condition, implying a 20-fold enhancement of the radiative

efficiency in full devices due to the HTL passivation alone. Alongside their hole transport layer strategy, the authors employed a sputtered indium zinc oxide interconnection layer (4 nm) between the two cells and a phenethylammonium iodide treatment between the perovskite and electron transporting layer (Fig. 5f). With a $\text{FA}_{0.75}\text{Cs}_{0.25}\text{Pb}(\text{I}_{0.6}\text{Br}_{0.4})_3$ perovskite ($E_g = 1.79$ eV) in small-area tandem devices (0.08 cm²) this resulted in a PCE of 23.60% (certified 22.95%) and a V_{OC} of 2.06 V and in large area devices (1.05 cm²) a PCE of 21.77% and V_{OC} of 2.06 V (Fig.4g).

The benefits from interfacial passivation can be dual fold: defect passivation and/or (in some cases) modification of the perovskite interface to improve energy alignment with a charge transport layer. Due to the lower number of tandem works reported employing methylammonium-free wide bandgap top cells there is still considerable scope for the exploration of various promising interfacial passivation additives, particularly those which have demonstrated success in methylammonium containing top cells in perovskite tandem devices (e.g. piperazinium iodide and similar molecules^{1,127}). It is worth noting that many interfacial passivation strategies do not improve operational stability of devices. Additionally, some passivation strategies (such as the use of phenethylammonium salts) can accelerate device degradation at elevated temperatures.¹²⁸ It is our opinion that passivation treatments which improve device operational stability should be prioritised. However, understanding the chemical interactions of passivation agents and how they influence device operational is crucial, both when the impact of this passivation is beneficial and detrimental to operational stability. This knowledge will ensure the continued advancement of operational stability across perovskite photovoltaics.

Optimisation of charge transport layers

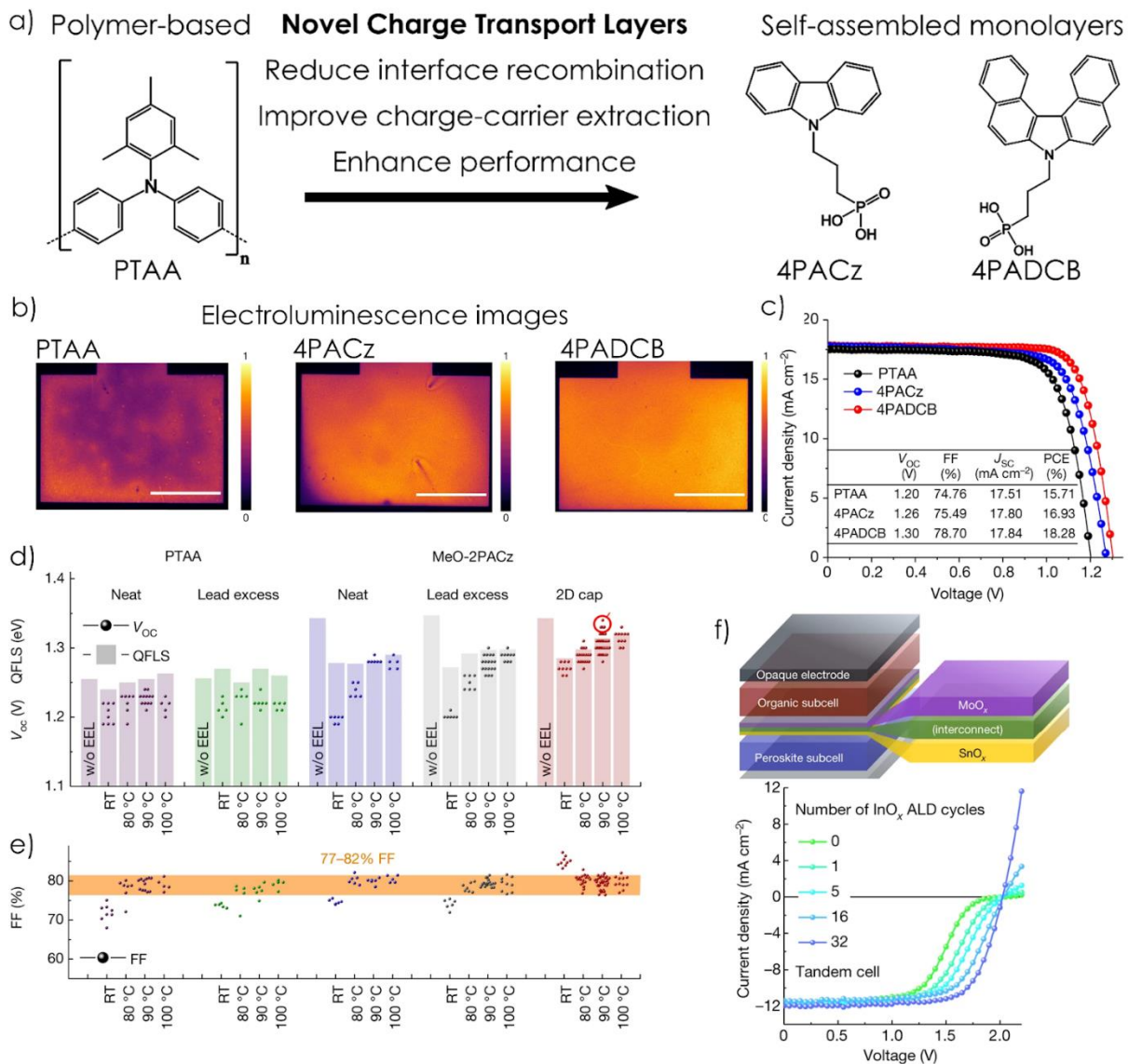


Figure 6 - Novel charge transport layers. a) Schematic describing the recent trend away from polymeric CTLs, towards those based on self-assembled monolayers (SAMs). SAM-based transport layers tend to reduce interface recombination, improve charge-carrier extraction and lead to substantially higher device performance. b) Electroluminescence images of complete devices, active area 1.044 cm^2 , based on $\text{FA}_{0.8}\text{Cs}_{0.2}\text{Pb}(\text{I}_{0.6}\text{Br}_{0.4})_3$ for different hole transport layers. The novel SAM-based device shows the highest and most uniform EL intensity indicative of reduced interfacial recombination at the perovskite/HTL interface. Scale bar is 0.5 cm . c) $J-V$ characteristics of all-perovskite 2T tandem solar cells where the wide bandgap subcell has differing HTLs, showing that implementing 4PADCB leads to a substantial boost in all device parameters. d) Comparison of the open-circuit voltage of complete perovskite solar cells, shown as dots, with the corresponding quasi-Fermi level splitting of representative layer stacks with PTAA or MeO-2PACz as the hole transport layers. The comparison for various device-annealing temperatures and benchmarked against the case with no electron extraction layer (w/o EEL). e) The FF is compared across the different annealing conditions, and different hole transport layers. The different temperatures refer to the annealing conditions after deposition of the AZO NP layer. f) Schematic of a perovskite–organic tandem cell, highlighted the interconnection layer. The $J-V$ characteristics of tandem cells

with varied thickness (number of ALD cycles) of the InO_x interconnection layer, showing Ohmic contact after 32 ALD cycles (~1.5 nm). Panels b-c adapted from ref.¹²⁹ Panels d-f adapted from ref.⁷⁹

Whilst several different charge transport layers have been employed in methylammonium-free wide bandgap tandem photovoltaic devices there is still considerable scope for investigation of alternative charge transport layers. Understanding and optimising the electronic structure at these interfaces will be instrumental in overcoming the voltage losses inhibiting device performances. Indeed, recent developments in methylammonium-free tandem devices can be attributed, at least in part, to improved energetic alignment between the valence and conduction band of the perovskite and that of the respective charge transport layers facilitating reductions in voltage losses and optimising the efficiency of these tandem devices.^{78,129} The understanding of the electronic structure, and therefore the energy level positions, of metal halide perovskite materials has proven incredibly challenging and is an area in which there is still more work to be done. For a thorough discussion of the challenges and developments in this area we recommend the following papers.^{130,131} Aside from the fundamental challenges associated with the measurements themselves, the number of different perovskite compositions and processing and chemical routes through which they are fabricated further compound this problem. It has been demonstrated that different chemical and processing routes result in perovskite materials with differing surface chemistries and therefore electronic structures.^{132–134} Additionally, the energy level positions of perovskite thin films have been demonstrated to be substrate dependent, therefore it is essential that this is considered when using energy level positions from literature reports to construct energy level alignment diagrams.^{135,136}

In the early stages of perovskite-on-Si tandem development significant progress was made in the optimisation of the perovskite top-cell architecture from *n-i-p* architectures to *p-i-n* architectures and then the subsequent optimisation of charge transport layers. Bush and co-workers employed evaporated C₆₀ as the electron transport layer with a SnO_x and zinc tin oxide (ZTO) buffer layer deposited by atomic layer deposition (ALD) or pulsed-chemical vapour deposition (CVD), followed by sputter coated ITO.¹³⁷ This was a significant improvement upon previous top contacts in perovskite-on-silicon tandem cells, which employed a thick hole conducting layer of spiro-OMeTAD and buffer layers of either ITO nanoparticles or thermally evaporated MoO_x prior to the ITO layer. The use of a C₆₀ and transparent metal oxide electron transporting layer has since become somewhat ubiquitous for use as the electron transport layer across the many different perovskite tandem devices.^{63,64,72,78,138} Fullerenes, like C₆₀, and their derivatives PC₆₁BM (phenyl-C₆₁-butyric-acid-methyl ester), PC₇₁BM (phenyl-C₇₁-butyric-acid-methyl ester), and ICBA (indene-C₆₀ bis-adduct), are widely employed in all types of metal halide perovskite photovoltaic devices. It is well known in the field of organic photovoltaics that energetic disorder, which can be dynamic or static, is an important cause of voltage losses in organic solar cells.¹³⁹ Whilst dynamic disorder is an inherent property of the semiconductor itself static disorder is a result of the crystallographic

packing of organic semiconducting molecules and therefore can be influenced by the thin film growth. It has been shown that fullerene derivatives such as PC₆₁BM and PC₇₁BM have a far larger degree of static disorder, relative to dynamic disorder, than their fullerene counterparts, C₆₀ and C₇₀.¹⁴⁰ Furthermore PC₇₁BM has an energetic disorder almost a third higher than two non-fullerene acceptors commonly used in organic PV.¹⁴¹ Understanding the role of disorder in voltage losses, if any, may prove important to maximise performance when using fullerenes as a charge transport layer in perovskite tandem photovoltaics. Additionally, we believe that there is considerable scope for successful implementation of non-fullerene acceptors, as we have seen in narrower bandgap perovskite photovoltaics.^{142–144} This may prove one such route to further minimise voltage losses, and boost performance in methylammonium-free wide bandgap tandem photovoltaics.

Despite the widespread use of C₆₀ in *p-i-n* devices there are often considerable voltage losses associated with its implementation as an electron transporting layer. Recent work, from Chen and co-workers focussed on understanding and overcoming these losses through an interfacial passivation route. Through a combined experimental and theoretical approach, they comprehensively studied the interface between C₆₀ and a 1.79 eV FA_{0.8}CS_{0.2}Pb(I_{0.6}Br_{0.4})₃ perovskite (suitable for all-perovskite tandem devices) and determined the associated voltage losses to be a result of poor energetic alignment and inhomogeneous surface potential at this interface. From this the authors introduced a diammonium passivation molecule (1,3-propane diammonium) which they determined significantly reduced the voltage losses in single junction devices and achieved an impressive, certified V_{oc} of 1.33V for their 1.79 eV perovskite. The authors conclude that this is due to the improvement in surface homogeneity and improved energetic alignment resulting from the passivation. Interestingly, unlike previous reports their structural investigations show that the implementation of this diammonium cation did not result in any changes to the perovskite structure.^{145,146} In 2-T all perovskite tandems this passivation enabled a PCE of 27.4% (26.29% certified) and a V_{oc} of 2.13 V for a device area of 0.049 cm² though we note similar device performances are also reported for areas of 1 cm².

Whilst several reports of perovskite tandems have utilised commercially available conductive polymers (e.g. PTAA, polyTPD, PFN-Br) recently significant developments have been made through the implementation of novel conductive polymer transport layers (Fig. 6a).^{83,89,147} Recently, mimicking their success in single junctions, there have been successful reports implementing “self-assembled monolayers” (SAMs) as the hole transporting layers in the wide bandgap cell of tandem devices.^{148,149} He and co-workers developed a new SAM (4-(7H-dibenzo[c,g]carbazol-7-yl)butyl)phosphonic acid (4PADCB) as the hole transporting layer for the wide bandgap cell in all-perovskite tandems.¹²⁹ He and co-workers employed molecular dynamics simulations to study existing charge transport layers and to aid in their development of these new SAM molecules, with an aim of synthesising molecules with an increased dipole moment. Photoluminescence and electroluminescence studies (Fig. 6b) of these new charge transporting materials in single junction devices demonstrated significant improvements in their ability to extract holes with fewer interfacial traps. With this novel molecule the authors report an impressive

reduction in V_{OC} losses (Fig. 6c), achieving 1.31 V in single junction devices with their absorber, $FA_{0.8}Cs_{0.2}Pb(I_{0.6}Br_{0.4})_3$ ($E_g = 1.77$ eV). When incorporated in 2-T all-perovskite tandems they achieved a PCE of 27.0% (26.4% certified steady-state) and a V_{OC} of 2.12 V for a device area of 1.044 cm².

Brinkmann and co-workers similarly demonstrated the implementation of a different self-assembled monolayer, MeO-2PACz ([2-(3,6-Dimethoxy-9H-carbazol-9-yl)ethyl]phosphonic acid), as the hole transporting layer of the wide bandgap cell in perovskite-organic tandem devices.⁷⁹ As part of their work developing these tandem devices, Brinkmann and co-workers used QFLS analysis in combination with device characterisation to study a broad range of materials and fabrication processes (Fig. 6d-e). Alongside their comprehensive investigation of the perovskite cell, which they consequently used to optimise its performance, they developed a novel interconnection layer based on ALD InO_x (Fig. 5f) to couple the perovskite and organic cells. This approach enabled impressive device performances utilising a $FA_{0.8}Cs_{0.2}Pb(I_{0.5}Br_{0.5})_3$ ($E_g = 1.85$ eV) perovskite, reporting 2-T devices with a PCE of 24.0 % (23.1% certified) and a V_{OC} of 2.15 V for a device area of 0.0174cm².

Operational stability of methylammonium-free metal halide perovskite tandem photovoltaics

Ensuring the long-term, operational stability of any metal halide perovskite photovoltaic technology will be critically important to ensuring their successful real-world deployment. This review is motivated by the belief of the authors that fully methylammonium-free compositions are among the most operationally stable perovskite photovoltaics. However, as we outline below, there is still considerable work to be done to determine which perovskite compositions will be most suitable for real-world applications.

The degradation of perovskite photovoltaics can be induced by exposure to light (visible and ultraviolet),¹⁵⁰ high temperatures,^{23,151} ambient environment (humidity, oxygen),^{152,153} electrical bias,¹⁵⁴ and chemical instabilities¹⁵⁵. It has been well established that perovskite photovoltaics which employ methylammonium as the sole A-site cation suffer from both light and heat induced degradation.^{150,156} In compositions which are methylammonium-free or contain small amounts of methylammonium there is no clear consensus on operational stability which can be directly related to the chemical composition of the perovskite. Some studies have suggested that a small amount of methylammonium can be beneficial to stability¹⁵⁷. Additionally, it remains unclear if post-deposition annealing of perovskites leads to elimination of methylammonium.¹⁵⁸ The stability of perovskite semiconductors is closely related to their defect density which can be influenced by their growth mechanism.^{159,160} Relatedly, there is strong evidence to suggest that the heterogeneity of the perovskite semiconductor can result in instabilities within photovoltaic devices.^{161,162} Therefore, in-depth stability studies must be performed on systems where the growth of each perovskite composition has been optimised to ensure that our understanding of stability is not clouded by heterogeneities and/or defects induced by unoptimised perovskite semiconductor growth.

We have predominantly focussed our discussion in this review on the performance of the devices highlighted, and only briefly discussed stability. This is due in part to the large variations in the conditions used for operational stability testing across the works discussed. These variations make comparisons and identifying meaningful trends difficult. We outline the conditions used for any operational stability data available in Supplementary Table 1 alongside information on both the single junction and tandem devices reported.

It is clear that to ascertain the stability of methylammonium-free wide bandgap based tandems more operational stability data is required, however determining which tests to undertake is not easy. Whilst conventional photovoltaics have well established qualification tests to ensure the longevity of their field performance, emerging photovoltaic technologies like those discussed in this review cannot be assessed using these tests due to the significant differences in degradation mechanisms and device architectures. At present, we have a range of tests recommended to assess the stability of perovskite photovoltaics based on the International Summit on Organic PV Stability (ISOS) protocols. We recommend the report from Khenkin and co-workers for an in-depth discussion on these tests.¹⁶³ At present, it is not clear which of these tests (if any) are truly representative of real-world deployment of perovskite photovoltaics. Until we know which testing parameters are required for a 25-year stable module we recommend that the field focuses on understanding the mechanisms that result in device degradation rather than aiming for long T80 lifetimes. For a comprehensive overview of long-term stability in perovskite photovoltaics we recommend the following review by Zhu and co-workers.¹⁶⁴

We would also like to note here that due to the significant time and infrastructure commitments required to fabricate any tandem device, it is often not possible to produce the same number of devices (and therefore have large statistical data) as with single junction devices. In the case of perovskite-on-Si tandems perhaps this is less important (as the stability of the silicon bottom cell is well established), but for other tandem architectures such as all-perovskite tandems large data sets of operational stability data would be incredibly valuable. This is an area where it would be of great benefit for us, as a research field, to use unified operational stability testing protocols to further our understanding of the stability of these devices.

Outlook and challenges

The impressive developments in the field of methylammonium-free wide bandgap photovoltaics in recent years have resulted in significant improvements in tandem device efficiency across both small and large area devices. Despite this there is still room for reduction in voltage losses, performance of large area devices, and device stability under accelerated aging conditions. We believe the key areas for continued development are as follows.

1. Minimising voltage losses through the development of improved fabrication routes and charge transport layers.

Whilst the majority of work in the wide-bandgap methylammonium-free device community has focussed on solution deposition there have been some reports of wide bandgap photovoltaic devices

based on evaporated methylammonium-free perovskites.¹⁶⁵ Whilst a broad range of approaches have been reported towards developing high performance methylammonium-free wide bandgap perovskite photovoltaics, it is clear that there is still considerable scope for reducing voltage losses and boosting not only the efficiency but the stability of these devices. For instance, world record open-circuit voltages for 1.8 eV perovskites stand at ~ 1.33 V. This corresponds to an EQE-EL of only $\sim 0.12\%$. When we can increase the EQE-EL to 10%, comparable to today's world record narrow bandgap perovskite cells, a V_{oc} as high as 1.45 V will be achieved. In the process of reviewing the literature several approaches have emerged which we believe the community should focus on to make gains in this area. Firstly, we believe it is essential that further effort is dedicated to investigating alternative charge transport layers which have been designed specifically for wide bandgap perovskites. In this review we have detailed several works demonstrating that considerable voltage losses can be mitigated through implementation of alternative charge transport layers. Ideally, these novel transport layers would be multifunctional: they would ensure good energetic alignment with the perovskite semiconductor, they would be selective to a specific charge-carrier and they need to promote homogenous perovskite thin-film growth. This latter requirement is essential to overcome the more complex crystallisation process present within mixed halide perovskites and reduce the likelihood of light induced halide segregation due to poor crystallinity. Additionally, there is a lack of understanding of the electronic structure of wide bandgap perovskites and therefore the energetic alignment of these materials with charge transport layers. This will require in-depth and systematic investigation, but we firmly believe that a more comprehensive understanding in this area will yield impressive results in reducing the voltage losses, which should not be considered inherent to these materials. Secondly, there have only been a very small number of reports detailing the evaporation of the methylammonium-free wide bandgap perovskite materials.¹⁶⁵ A large part of the reason for the dearth in reports on vapour deposited perovskite cells, is that it takes more money and time to establish thermal evaporation capacity at the research scale. However, with many groups now having equipment in place for thermal evaporation, coupled with the inherent advantages for depositing conformal coatings on textured surfaces and without the requirement for the use of harmful solvents, we expect to observe significant progress with vapour deposited wide bandgap perovskites over the next few years.

2. Identification of the degradation failure mechanisms within devices

Stability is a key hurdle to be overcome on the path towards commercial implementation of perovskite photovoltaic devices. Whilst this review highlights many promising results and approaches towards enhancing the efficiency and stability of methylammonium-free wide bandgap perovskite photovoltaics there are still considerable gaps in our understanding of the long-term stability of perovskite photovoltaic devices under harsh accelerated aging conditions. In our view, stress tests in an academic environment should be performed to discover failure modes, or to assess if some mode of stability is impacted by a given change in the recipe or chemistry.^{166–169} Stress tests should not be performed to demonstrate that a given recipe or chemistry is stable, since the latter encourages stressing under mild conditions and will not lead to rapid advances in understanding and

meaningful advances in long term stability. There are a broad range of different stress conditions reported in the international summit of organic solar cells (ISOS) protocols consensus statement for perovskite solar cell stress tests.¹⁶³ However, we strongly encourage the field to undertake more aggressive stability testing, in air and in high humidity environments without the use of encapsulation. Accelerated aging of encapsulated devices, can often become a test of how good the encapsulation approach is rather than an assessment of the inherent stability of the perovskite device. We would like to see aggressive stability testing more widely reported, and as a major focus of studies e.g. light soaking under elevated temperatures of 85 °C or higher, rather than room temperature, damp heat stress tests at 85 °C and 85 % RH, and ideally combining multiple harsh stress conditions in the presence of light, to understand the full impact of interface modifications on long-term device stability. From reviewing the literature, several important trends emerged that result in durable wide bandgap perovskite solar cells: it is critical to form homogenous perovskite thin films which can be achieved through a combination of process optimisation, additive engineering and/or improved charge transport layers; the inclusion of additives into the precursor solution, e.g. ionic additives⁶⁶, which have shown to result in a dramatic increase in stability; and the development of more stable transport layers in the durability of the entire device stack, not just the perovskite, that determines the operational lifetime. Reviewers and editors should also appreciate that the degradation rate is expected to approximately double, with every 10 °C raise in stressing temperature, when comparing between different published works.^{170,171}

3. Continued moving beyond developments in individual research labs to broad developments across the research community

It is important to note that a small number of research groups are responsible for a large number of the papers cited in this review. This is due in large part to the expensive infrastructure required to fabricate and characterize highly efficient methylammonium-free wide bandgap tandem devices. This delays potential developments as a large fraction of the community are inhibited from working in these areas. Whilst, as a community, we collaborate and share results widely there are still efforts we can take to widen the pool of researchers able to work on tandem devices and accelerate developments in this area. In Europe the Horizon 2020 project VIPERLAB enables researchers to apply for access to carry out experiments using the extensive infrastructure available across a range of institutions to carry out work on perovskite photovoltaics.¹⁷² More initiatives like this, available to researchers worldwide, will enable researchers from groups within the required infrastructure to contribute to the development of methylammonium-free perovskite tandem devices.

The open access perovskite database and analysis tool contains extensive information relating to the fabrication and characterisation of reported perovskite photovoltaic devices as well as device performance.¹⁷³ Although relatively new, this database has already proven to be an incredibly valuable resource for researchers in identifying potential routes to push forward perovskite photovoltaic device performance. The perovskite database is also incredibly useful for computational prediction methods, like machine and active learning approaches, in areas relating to

materials discovery and data analysis.^{174–176} The application of these types of models to perovskite photovoltaic device development and characterisation is a growth area and we predict will become incredibly important in the continued development of methylammonium-free wide bandgap perovskite tandem photovoltaics.

Acknowledgments

The authors acknowledge support from the European Union's Horizon 2020 research and innovation program under grant agreement no. 861985 (peroCUBE) and the UK's Engineering and Physical Sciences Research Council (EPSRC) EP/T025077/1 and EP/T012455/1. RDJO acknowledges the support of the Penrose Scholarship.

Competing Interests

H.J.S. is the co-founder and CSO of Oxford PV Ltd, a company that is commercialising perovskite photovoltaic technologies. A.J.R., R.D.J.O, and M.B.J. declare no competing interests.

References

1. Mariotti, S. *et al.* Interface engineering for high-performance, triple-halide perovskite–silicon tandem solar cells. *Science* **381**, 63–69 (2023).
2. Green, M. A. *et al.* Solar cell efficiency tables (Version 60). *Prog. Photovolt. Res. Appl.* **30**, 687–701.
3. Mitzi, D. B., Wang, S., Feild, C. A., Chess, C. A. & Guloy, A. M. Conducting Layered Organic-inorganic Halides Containing <110>-Oriented Perovskite Sheets. *Science* **267**, 1473–1476 (1995).
4. Wehrenfennig, C., Eperon, G. E., Johnston, M. B., Snaith, H. J. & Herz, L. M. High Charge Carrier Mobilities and Lifetimes in Organolead Trihalide Perovskites. *Adv. Mater.* **26**, 1584–1589 (2014).
5. Herz, L. M. Charge-Carrier Mobilities in Metal Halide Perovskites: Fundamental Mechanisms and Limits. *ACS Energy Lett.* **2**, 1539–1548 (2017).
6. Stranks, S. D. *et al.* Electron-Hole Diffusion Lengths Exceeding 1 Micrometer in an Organometal Trihalide Perovskite Absorber. *Science* **342**, 341–344 (2013).
7. Yang, Z. *et al.* Enhancing electron diffusion length in narrow-bandgap perovskites for efficient monolithic perovskite tandem solar cells. *Nat. Commun.* **10**, (2019).
8. Green, M. A., Jiang, Y., Soufiani, A. M. & Ho-Baillie, A. Optical Properties of Photovoltaic Organic–Inorganic Lead Halide Perovskites. *J. Phys. Chem. Lett.* **6**, 4774–4785 (2015).
9. De Wolf, S. *et al.* Organometallic Halide Perovskites: Sharp Optical Absorption Edge and Its Relation to Photovoltaic Performance. *J. Phys. Chem. Lett.* **5**, 1035–1039 (2014).

10. Liang, J. *et al.* Defect-Engineering-Enabled High-Efficiency All-Inorganic Perovskite Solar Cells. *Adv. Mater.* **31**, 1903448 (2019).
11. Ledinsky, M. *et al.* Temperature Dependence of the Urbach Energy in Lead Iodide Perovskites. *J. Phys. Chem. Lett.* **10**, 1368–1373 (2019).
12. Mehdizadeh-Rad, H. & Singh, J. Influence of Urbach Energy, Temperature, and Longitudinal Position in the Active Layer on Carrier Diffusion Length in Perovskite Solar Cells. *ChemPhysChem* **20**, 2712–2717 (2019).
13. Subedi, B. *et al.* Urbach Energy and Open-Circuit Voltage Deficit for Mixed Anion–Cation Perovskite Solar Cells. *ACS Appl. Mater. Interfaces* **14**, 7796–7804 (2022).
14. Unger, E. L. *et al.* Roadmap and roadblocks for the band gap tunability of metal halide perovskites. *J. Mater. Chem. A* **5**, 11401–11409 (2017).
15. Hörantner, M. T. *et al.* The Potential of Multijunction Perovskite Solar Cells. *ACS Energy Lett.* **2**, 2506–2513 (2017).
16. Lal, N. N., White, T. P. & Catchpole, K. R. Optics and Light Trapping for Tandem Solar Cells on Silicon. *IEEE J. Photovolt.* **4**, 1380–1386 (2014).
17. Tong, J. *et al.* Carrier lifetimes of >1 ms in Sn-Pb perovskites enable efficient all-perovskite tandem solar cells. *Science* **364**, 475–479 (2019).
18. Hu, S. *et al.* Optimized carrier extraction at interfaces for 23.6% efficient tin–lead perovskite solar cells. *Energy Environ. Sci.* **15**, 2096–2107 (2022).
19. Slotcavage, D. J., Karunadasa, H. I. & McGehee, M. D. Light-Induced Phase Segregation in Halide-Perovskite Absorbers. *ACS Energy Lett.* **1**, 1199–1205 (2016).
20. Conings, B. *et al.* Structure–Property Relations of Methylamine Vapor Treated Hybrid Perovskite CH₃NH₃PbI₃ Films and Solar Cells. *ACS Appl. Mater. Interfaces* **9**, 8092–8099 (2017).
21. Tan, H. *et al.* Dipolar cations confer defect tolerance in wide-bandgap metal halide perovskites. *Nat. Commun.* **9**, 3100 (2018).
22. Jaysankar, M. *et al.* Minimizing Voltage Loss in Wide-Bandgap Perovskites for Tandem Solar Cells. *ACS Energy Lett.* **4**, 259–264 (2019).

23. Tan, W., Bowring, A. R., Meng, A. C., McGehee, M. D. & McIntyre, P. C. Thermal Stability of Mixed Cation Metal Halide Perovskites in Air. *ACS Appl. Mater. Interfaces* **10**, 5485–5491 (2018).
24. Chen, H. *et al.* Regulating surface potential maximizes voltage in all-perovskite tandems. *Nature* **613**, 676–681 (2023).
25. Lin, R. *et al.* All-perovskite tandem solar cells with 3D/3D bilayer perovskite heterojunction. *Nature* 1–3 (2023) doi:10.1038/s41586-023-06278-z.
26. Jiang, Q. *et al.* Compositional texture engineering for highly stable wide-bandgap perovskite solar cells. *Science* **378**, 1295–1300 (2022).
27. Ji, K., Anaya, M., Abfalterer, A. & Stranks, S. D. Halide Perovskite Light-Emitting Diode Technologies. *Adv. Opt. Mater.* **9**, 2002128 (2021).
28. Ren, Z., Wang, K., Sun, X. W. & Choy, W. C. H. Strategies Toward Efficient Blue Perovskite Light-Emitting Diodes. *Adv. Funct. Mater.* **31**, 2100516 (2021).
29. Yang, D. *et al.* Toward Stable and Efficient Perovskite Light-Emitting Diodes. *Adv. Funct. Mater.* **32**, 2109495 (2022).
30. Liang, X. *et al.* Promoting Energy Transfer Between Quasi-2D Perovskite Layers Toward Highly Efficient Red Light-Emitting Diodes. *Small* **18**, 2204638 (2022).
31. Liu, Y. *et al.* Boosting the efficiency of quasi-2D perovskites light-emitting diodes by using encapsulation growth method. *Nano Energy* **80**, 105511–105511 (2021).
32. Warby, J. H. *et al.* Revealing Factors Influencing the Operational Stability of Perovskite Light-Emitting Diodes. *ACS Nano* **14**, 8855–8865 (2020).
33. Stranks, S. D., Hoyer, R. L. Z., Di, D., Friend, R. H. & Deschler, F. The Physics of Light Emission in Halide Perovskite Devices. *Adv. Mater.* **31**, 1803336 (2019).
34. Wang, Z. *et al.* Manipulating the Trade-off Between Quantum Yield and Electrical Conductivity for High-Brightness Quasi-2D Perovskite Light-Emitting Diodes. *Adv. Funct. Mater.* **28**, 1804187 (2018).
35. Caprioglio, P. *et al.* On the Relation between the Open-Circuit Voltage and Quasi-Fermi Level Splitting in Efficient Perovskite Solar Cells. *Adv. Energy Mater.* **9**, 1901631–1901631 (2019).

36. Krückemeier, L., Rau, U., Stolterfoht, M. & Kirchartz, T. How to Report Record Open-Circuit Voltages in Lead-Halide Perovskite Solar Cells. *Adv. Energy Mater.* **10**, 1902573–1902573 (2020).
37. Nayak, P. K., Mahesh, S., Snaith, H. J. & Cahen, D. Photovoltaic solar cell technologies: analysing the state of the art. *Nat. Rev. Mater.* **4**, 269–285 (2019).
38. Rau, U., Blank, B., Müller, T. C. M. & Kirchartz, T. Efficiency Potential of Photovoltaic Materials and Devices Unveiled by Detailed-Balance Analysis. *Phys. Rev. Appl.* **7**, 044016–044016 (2017).
39. Green, M. A. & Ho-Baillie, A. W. Y. Pushing to the Limit: Radiative Efficiencies of Recent Mainstream and Emerging Solar Cells. *ACS Energy Lett.* **4**, 1639–1644 (2019).
40. Almora, O. *et al.* Quantifying the Absorption Onset in the Quantum Efficiency of Emerging Photovoltaic Devices. *Adv. Energy Mater.* **11**, 2100022 (2021).
41. Mahesh, S. *et al.* Revealing the origin of voltage loss in mixed-halide perovskite solar cells. *Energy Environ. Sci.* **13**, 258–267 (2020).
42. Caprioglio, P. *et al.* Nano-emitting Heterostructures Violate Optical Reciprocity and Enable Efficient Photoluminescence in Halide-Segregated Methylammonium-Free Wide Bandgap Perovskites. *ACS Energy Lett.* **6**, 419–428 (2021).
43. Yang, W. *et al.* Unlocking Voltage Potentials of Mixed-Halide Perovskite Solar Cells via Phase Segregation Suppression. *Adv. Funct. Mater.* **32**, 2110698 (2022).
44. Knight, A. J. & Herz, L. M. Preventing phase segregation in mixed-halide perovskites: a perspective. *Energy Environ. Sci.* **13**, 2024–2046 (2020).
45. Barker, A. J. *et al.* Defect-Assisted Photoinduced Halide Segregation in Mixed-Halide Perovskite Thin Films. *ACS Energy Lett.* **2**, 1416–1424 (2017).
46. Yoon, S. J. *et al.* Tracking Iodide and Bromide Ion Segregation in Mixed Halide Lead Perovskites during Photoirradiation. *ACS Energy Lett.* **1**, 290–296 (2016).
47. Motti, S. G. *et al.* Phase segregation in mixed-halide perovskites affects charge-carrier dynamics while preserving mobility. *Nat. Commun.* **12**, 6955 (2021).
48. Peña-Camargo, F. *et al.* Halide Segregation versus Interfacial Recombination in Bromide-Rich Wide-Gap Perovskite Solar Cells. *ACS Energy Lett.* **5**, 2728–2736 (2020).

49. Wang, Z. *et al.* Suppressed phase segregation for triple-junction perovskite solar cells. *Nature* 1–3 (2023) doi:10.1038/s41586-023-06006-7.
50. Zhou, Y., Poli, I., Meggiolaro, D., De Angelis, F. & Petrozza, A. Defect activity in metal halide perovskites with wide and narrow bandgap. *Nat. Rev. Mater.* **6**, 986–1002 (2021).
51. J. Oliver, R. D. *et al.* Understanding and suppressing non-radiative losses in methylammonium-free wide-bandgap perovskite solar cells. *Energy Environ. Sci.* **15**, 714–726 (2022).
52. Motti, S. G. *et al.* Defect Activity in Lead Halide Perovskites. *Adv. Mater.* **31**, 1901183 (2019).
53. Long, M. *et al.* Abnormal Synergetic Effect of Organic and Halide Ions on the Stability and Optoelectronic Properties of a Mixed Perovskite via In Situ Characterizations. *Adv. Mater.* **30**, 1801562–1801562 (2018).
54. Fu, F. *et al.* I₂ vapor-induced degradation of formamidinium lead iodide based perovskite solar cells under heat–light soaking conditions. *Energy Environ. Sci.* **12**, 3074–3088 (2019).
55. Motti, S. G. *et al.* Controlling competing photochemical reactions stabilizes perovskite solar cells. *Nat. Photonics* **13**, 532–539 (2019).
56. Cho, H. *et al.* Overcoming the electroluminescence efficiency limitations of perovskite light-emitting diodes. *Science* **350**, 1222–1225 (2015).
57. Meggiolaro, D., Mosconi, E. & De Angelis, F. Formation of Surface Defects Dominates Ion Migration in Lead-Halide Perovskites. *ACS Energy Lett.* **4**, 779–785 (2019).
58. Albrecht, S. *et al.* Towards optical optimization of planar monolithic perovskite/silicon-heterojunction tandem solar cells. *J. Opt.* **18**, 064012 (2016).
59. Filipič, M. *et al.* CH₃NH₃PbI₃ perovskite / silicon tandem solar cells: characterization based optical simulations. *Opt. Express* **23**, A263–A278 (2015).
60. Werner, J. *et al.* Efficient Near-Infrared-Transparent Perovskite Solar Cells Enabling Direct Comparison of 4-Terminal and Monolithic Perovskite/Silicon Tandem Cells. *ACS Energy Lett.* **1**, 474–480 (2016).
61. Hörantner, M. T. & Snaith, H. J. Predicting and optimising the energy yield of perovskite-on-silicon tandem solar cells under real world conditions. *Energy Environ. Sci.* **10**, 1983–1993 (2017).

62. Ho-Baillie, A. W. Y. *et al.* Recent progress and future prospects of perovskite tandem solar cells. *Appl. Phys. Rev.* **8**, 041307 (2021).
63. Sahli, F. *et al.* Fully textured monolithic perovskite/silicon tandem solar cells with 25.2% power conversion efficiency. *Nat. Mater.* **17**, 820–826 (2018).
64. Li, Y. *et al.* Wide Bandgap Interface Layer Induced Stabilized Perovskite/Silicon Tandem Solar Cells with Stability over Ten Thousand Hours. *Adv. Energy Mater.* **11**, 2102046–2102046 (2021).
65. Al-Ashouri, A. *et al.* Monolithic perovskite/silicon tandem solar cell with >29% efficiency by enhanced hole extraction. *Science* **370**, 1300–1309 (2020).
66. Lin, Y.-H. *et al.* A piperidinium salt stabilizes efficient metal-halide perovskite solar cells. *Science* **369**, 96–102 (2020).
67. Mazzarella, L. *et al.* Infrared Light Management Using a Nanocrystalline Silicon Oxide Interlayer in Monolithic Perovskite/Silicon Heterojunction Tandem Solar Cells with Efficiency above 25%. *Adv. Energy Mater.* **9**, 1803241 (2019).
68. Eperon, G. E., Hörantner, M. T. & Snaith, H. J. Metal halide perovskite tandem and multiple-junction photovoltaics. *Nat. Rev. Chem.* **1**, 1–18 (2017).
69. Im, J., Stoumpos, C. C., Jin, H., Freeman, A. J. & Kanatzidis, M. G. Antagonism between Spin–Orbit Coupling and Steric Effects Causes Anomalous Band Gap Evolution in the Perovskite Photovoltaic Materials $\text{CH}_3\text{NH}_3\text{Sn}_{1-x}\text{Pb}_x\text{I}_3$. *J. Phys. Chem. Lett.* **6**, 3503–3509 (2015).
70. Eperon, G. E. *et al.* Perovskite-perovskite tandem photovoltaics with optimized band gaps. *Science* **354**, 861–865 (2016).
71. Yang, Z. *et al.* Stable Low-Bandgap Pb–Sn Binary Perovskites for Tandem Solar Cells. *Adv. Mater.* **28**, 8990–8997 (2016).
72. Lin, R. *et al.* Monolithic all-perovskite tandem solar cells with 24.8% efficiency exploiting comproportionation to suppress Sn(II) oxidation in precursor ink. *Nat. Energy* **4**, 864–873 (2019).
73. Moot, T. *et al.* Choose Your Own Adventure: Fabrication of Monolithic All-Perovskite Tandem Photovoltaics. *Adv. Mater.* **32**, 2003312 (2020).

74. Zhang, M. *et al.* Single-layered organic photovoltaics with double cascading charge transport pathways: 18% efficiencies. *Nat. Commun.* **12**, 309 (2021).
75. Yao, H., Wang, J., Xu, Y., Zhang, S. & Hou, J. Recent Progress in Chlorinated Organic Photovoltaic Materials. *Acc. Chem. Res.* **53**, 822–832 (2020).
76. Yuan, J. *et al.* Single-Junction Organic Solar Cell with over 15% Efficiency Using Fused-Ring Acceptor with Electron-Deficient Core. *Joule* **3**, 1140–1151 (2019).
77. McMeekin, D. P. *et al.* Solution-Processed All-Perovskite Multi-junction Solar Cells. *Joule* **3**, 387–401 (2019).
78. Chen, W. *et al.* Monolithic perovskite/organic tandem solar cells with 23.6% efficiency enabled by reduced voltage losses and optimized interconnecting layer. *Nat. Energy* **7**, 229–237 (2022).
79. Brinkmann, K. O. *et al.* Perovskite–organic tandem solar cells with indium oxide interconnect. *Nature* **604**, 280–286 (2022).
80. Xiao, K. *et al.* Solution-Processed Monolithic All-Perovskite Triple-Junction Solar Cells with Efficiency Exceeding 20%. *ACS Energy Lett.* **5**, 2819–2826 (2020).
81. Zheng, J. *et al.* Monolithic Perovskite–Perovskite–Silicon Triple-Junction Tandem Solar Cell with an Efficiency of over 20%. *ACS Energy Lett.* **7**, 3003–3005 (2022).
82. Werner, J. *et al.* Perovskite/Perovskite/Silicon Monolithic Triple-Junction Solar Cells with a Fully Textured Design. *ACS Energy Lett.* **3**, 2052–2058 (2018).
83. Xiao, K. *et al.* Scalable processing for realizing 21.7%-efficient all-perovskite tandem solar modules. *Science* **376**, 762–767 (2022).
84. Vaynzof, Y. The Future of Perovskite Photovoltaics—Thermal Evaporation or Solution Processing? *Adv. Energy Mater.* **10**, 2003073 (2020).
85. McMeekin, D. P. *et al.* A mixed-cation lead mixed-halide perovskite absorber for tandem solar cells. *Science* **351**, 151–155 (2016).
86. Yu, F. *et al.* Efficient and Stable Wide-Bandgap Perovskite Solar Cells Derived from a Thermodynamic Phase-Pure Intermediate. *Sol. RRL* **6**, 2100906–2100906 (2022).

87. Zhou, Y. *et al.* Composition-Tuned Wide Bandgap Perovskites: From Grain Engineering to Stability and Performance Improvement. *Adv. Funct. Mater.* **28**, 1803130–1803130 (2018).
88. Yu, Y. *et al.* Synergistic Effects of Lead Thiocyanate Additive and Solvent Annealing on the Performance of Wide-Bandgap Perovskite Solar Cells. *ACS Energy Lett.* **2**, 1177–1182 (2017).
89. Wen, J. *et al.* Steric Engineering Enables Efficient and Photostable Wide-Bandgap Perovskites for All-Perovskite Tandem Solar Cells. *Adv. Mater.* **34**, 2110356 (2022).
90. Bush, K. A. *et al.* Compositional Engineering for Efficient Wide Band Gap Perovskites with Improved Stability to Photoinduced Phase Segregation. *ACS Energy Lett.* **3**, 428–435 (2018).
91. Bush, K. A. *et al.* Minimizing Current and Voltage Losses to Reach 25% Efficient Monolithic Two-Terminal Perovskite–Silicon Tandem Solar Cells. *ACS Energy Lett.* **3**, (2018).
92. Li, R. *et al.* CsPbCl₃-Cluster-Widened Bandgap and Inhibited Phase Segregation in a Wide-Bandgap Perovskite and its Application to NiO_x-Based Perovskite/Silicon Tandem Solar Cells. *Adv. Mater.* **34**, 2201451 (2022).
93. Noel, N. K. *et al.* Unveiling the Influence of pH on the Crystallization of Hybrid Perovskites, Delivering Low Voltage Loss Photovoltaics. *Joule* **1**, 328–343 (2017).
94. Marshall, A. R. *et al.* Dimethylammonium: An A-Site Cation for Modifying CsPbI₃. *Sol. RRL* **5**, 2000599 (2021).
95. Ke, W., Spanopoulos, I., Stoumpos, C. C. & Kanatzidis, M. G. Myths and reality of HPbI₃ in halide perovskite solar cells. *Nat. Commun.* **9**, 4785 (2018).
96. McMeekin, D. P. *et al.* Crystallization Kinetics and Morphology Control of Formamidinium–Cesium Mixed-Cation Lead Mixed-Halide Perovskite via Tunability of the Colloidal Precursor Solution. *Adv. Mater.* **29**, 1607039 (2017).
97. Abdi-Jalebi, M. *et al.* Maximizing and stabilizing luminescence from halide perovskites with potassium passivation. *Nature* **555**, 497–501 (2018).
98. Tang, Z. *et al.* Hysteresis-free perovskite solar cells made of potassium-doped organometal halide perovskite. *Sci. Rep.* **7**, 12183–12183 (2017).

99. Nam, J. K. *et al.* Potassium Incorporation for Enhanced Performance and Stability of Fully Inorganic Cesium Lead Halide Perovskite Solar Cells. *Nano Lett.* **17**, 2028–2033 (2017).
100. Palmstrom, A. F. *et al.* Enabling Flexible All-Perovskite Tandem Solar Cells. *Joule* **3**, 2193–2204 (2019).
101. Huang, Z. *et al.* Stable, Bromine-Free, Tetragonal Perovskites with 1.7 eV Bandgaps via A-Site Cation Substitution. *ACS Mater. Lett.* **2**, 869–872 (2020).
102. Tan, S. *et al.* Steric Impediment of Ion Migration Contributes to Improved Operational Stability of Perovskite Solar Cells. *Adv. Mater.* **32**, 1906995 (2020).
103. Beal, R. E. *et al.* Cesium Lead Halide Perovskites with Improved Stability for Tandem Solar Cells. *J. Phys. Chem. Lett.* **7**, 746–751 (2016).
104. T. Hoke, E. *et al.* Reversible photo-induced trap formation in mixed-halide hybrid perovskites for photovoltaics. *Chem. Sci.* **6**, 613–617 (2015).
105. Brennan, M. C., Draguta, S., Kamat, P. V. & Kuno, M. Light-Induced Anion Phase Segregation in Mixed Halide Perovskites. *ACS Energy Lett.* **3**, 204–213 (2018).
106. Wang, L. *et al.* Strain Modulation for Light-Stable n–i–p Perovskite/Silicon Tandem Solar Cells. *Adv. Mater.* **34**, 2201315 (2022).
107. Guan, H. *et al.* Low-Dimensional 2-thiopheneethylammonium Lead Halide Capping Layer Enables Efficient Single-Junction Methylamine-Free Wide-Bandgap and Tandem Perovskite Solar Cells. *Adv. Funct. Mater.* **n/a**, 2300860.
108. Chen, C. *et al.* Interfacial engineering of a thiophene-based 2D/3D perovskite heterojunction for efficient and stable inverted wide-bandgap perovskite solar cells. *Nano Energy* **90**, 106608–106608 (2021).
109. Bai, S. *et al.* Planar perovskite solar cells with long-term stability using ionic liquid additives. *Nature* **571**, 245–250 (2019).
110. Caprioglio, P. *et al.* Bi-functional interfaces by poly(ionic liquid) treatment in efficient pin and nip perovskite solar cells. *Energy Environ. Sci.* **14**, 4508–4522 (2021).

111. Gharibzadeh, S. *et al.* Record Open-Circuit Voltage Wide-Bandgap Perovskite Solar Cells Utilizing 2D/3D Perovskite Heterostructure. *Adv. Energy Mater.* **9**, 1803699–1803699 (2019).
112. Noel, N. K. *et al.* Elucidating the Role of a Tetrafluoroborate-Based Ionic Liquid at the n-Type Oxide/Perovskite Interface. *Adv. Energy Mater.* **10**, 1903231 (2020).
113. Niu, T. *et al.* Ionic Liquids-Enabled Efficient and Stable Perovskite Photovoltaics: Progress and Challenges. *ACS Energy Lett.* **6**, 1453–1479 (2021).
114. Zhou, Y. *et al.* Benzylamine-Treated Wide-Bandgap Perovskite with High Thermal-Photostability and Photovoltaic Performance. *Adv. Energy Mater.* **7**, 1701048–1701048 (2017).
115. Wang, Z. *et al.* Efficient ambient-air-stable solar cells with 2D-3D heterostructured butylammonium-caesium-formamidinium lead halide perovskites. *Nat. Energy* **2**, 17135–17135 (2017).
116. Bu, T. *et al.* Structure engineering of hierarchical layered perovskite interface for efficient and stable wide bandgap photovoltaics. *Nano Energy* **75**, 104917 (2020).
117. Chen, C. *et al.* Arylammonium-Assisted Reduction of the Open-Circuit Voltage Deficit in Wide-Bandgap Perovskite Solar Cells: The Role of Suppressed Ion Migration. *ACS Energy Lett.* **5**, 2560–2568 (2020).
118. Chen, C. *et al.* Achieving a high open-circuit voltage in inverted wide-bandgap perovskite solar cells with a graded perovskite homojunction. *Nano Energy* **61**, 141–147 (2019).
119. Yang, D. *et al.* Surface optimization to eliminate hysteresis for record efficiency planar perovskite solar cells. *Energy Environ. Sci.* **9**, 3071–3078 (2016).
120. Wu, Y. *et al.* Thermally Stable MAPbI₃ Perovskite Solar Cells with Efficiency of 19.19% and Area over 1 cm² achieved by Additive Engineering. *Adv. Mater.* **29**, 1701073 (2017).
121. Wu, Q. *et al.* Solution-Processable Ionic Liquid as an Independent or Modifying Electron Transport Layer for High-Efficiency Perovskite Solar Cells. *ACS Appl. Mater. Interfaces* **8**, 34464–34473 (2016).
122. Zhang, F. & Zhu, K. Additive Engineering for Efficient and Stable Perovskite Solar Cells. *Adv. Energy Mater.* **10**, 1902579 (2020).

123. Gharibzadeh, S. *et al.* 2D/3D Heterostructure for Semitransparent Perovskite Solar Cells with Engineered Bandgap Enables Efficiencies Exceeding 25% in Four-Terminal Tandems with Silicon and CIGS. *Adv. Funct. Mater.* **30**, 1909919–1909919 (2020).
124. Grancini, G. *et al.* One-Year stable perovskite solar cells by 2D/3D interface engineering. *Nat. Commun.* **2017 81 8**, 1–8 (2017).
125. Katan, C., Mercier, N. & Even, J. Quantum and Dielectric Confinement Effects in Lower-Dimensional Hybrid Perovskite Semiconductors. *Chem. Rev.* **119**, 3140–3192 (2019).
126. Noel, N. K. *et al.* Enhanced Photoluminescence and Solar Cell Performance via Lewis Base Passivation of Organic–Inorganic Lead Halide Perovskites. *ACS Nano* **8**, 9815–9821 (2014).
127. Li, F. *et al.* Regulating Surface Termination for Efficient Inverted Perovskite Solar Cells with Greater Than 23% Efficiency. *J. Am. Chem. Soc.* **142**, 20134–20142 (2020).
128. Jiang, Q. *et al.* Surface passivation of perovskite film for efficient solar cells. *Nat. Photonics* **13**, 460–466 (2019).
129. He, R. *et al.* All-perovskite tandem 1 cm² cells with improved interface quality. *Nature* 1–3 (2023) doi:10.1038/s41586-023-05992-y.
130. Zu, F., Shin, D. & Koch, N. Electronic properties of metal halide perovskites and their interfaces: the basics. *Mater. Horiz.* **9**, 17–24 (2022).
131. Béchu, S., Ralaiarisoa, M., Etcheberry, A. & Schulz, P. Photoemission Spectroscopy Characterization of Halide Perovskites. *Adv. Energy Mater.* **10**, 1904007–1904007 (2020).
132. Ramadan, A. J. *et al.* Revealing the Stoichiometric Tolerance of Lead Trihalide Perovskite Thin Films. *Chem. Mater.* **32**, 114–120 (2020).
133. Ramadan, A. J. *et al.* Unravelling the Improved Electronic and Structural Properties of Methylammonium Lead Iodide Deposited from Acetonitrile. *Chem. Mater.* **30**, 7737–7743 (2018).
134. Ramadan, A. J., Rochford, L. A., Fearn, S. & Snaith, H. J. Processing Solvent-Dependent Electronic and Structural Properties of Cesium Lead Triiodide Thin Films. *J. Phys. Chem. Lett.* **8**, 4172–4176 (2017).
135. Olthof, S. & Meerholz, K. Substrate-dependent electronic structure and film formation of MAPbI₃ perovskites. *Sci. Rep.* **7**, 40267 (2017).

136. Canil, L. *et al.* Tuning halide perovskite energy levels. *Energy Environ. Sci.* **14**, 1429–1438 (2021).
137. Bush, K. A. *et al.* 23.6%-efficient monolithic perovskite/silicon tandem solar cells with improved stability. *Nat. Energy* **2**, (2017).
138. Yu, Z. *et al.* Simplified interconnection structure based on C60/SnO₂-x for all-perovskite tandem solar cells. *Nat. Energy* **5**, 657–665 (2020).
139. Jungbluth, A., Kaienburg, P. & Riede, M. Charge transfer state characterization and voltage losses of organic solar cells. *J. Phys. Mater.* **5**, 024002–024002 (2022).
140. Tummala, N. R., Zheng, Z., Aziz, S. G., Coropceanu, V. & Brédas, J.-L. Static and Dynamic Energetic Disorders in the C₆₀, PC61BM, C70, and PC71BM Fullerenes. *J. Phys. Chem. Lett.* **6**, 3657–3662 (2015).
141. Kupgan, G., Chen, X.-K. & Brédas, J.-L. Low Energetic Disorder in Small-Molecule Non-Fullerene Electron Acceptors. *ACS Mater. Lett.* **1**, 350–353 (2019).
142. Zhang, M. & Zhan, X. Nonfullerene n-Type Organic Semiconductors for Perovskite Solar Cells. *Adv. Energy Mater.* **9**, 1900860–1900860 (2019).
143. Song, C. *et al.* Sulfonyl-based non-fullerene electron acceptor-assisted grain boundary passivation for efficient and stable perovskite solar cells. *J. Mater. Chem. A* **7**, 19881–19888 (2019).
144. Yang, Q. *et al.* Hydroxylated non-fullerene acceptor for highly efficient inverted perovskite solar cells. *Energy Environ. Sci.* **14**, 6536–6545 (2021).
145. Zhang, L. *et al.* Surface Defect Passivation of Pb–Sn-Alloyed Perovskite Film by 1,3-Propanediammonium Iodide toward High-Performance Photovoltaic Devices. *Sol. RRL* **5**, 2100299 (2021).
146. Zhang, F. *et al.* Metastable Dion-Jacobson 2D structure enables efficient and stable perovskite solar cells. *Science* **375**, 71–76 (2022).
147. Wang, Y. *et al.* Cross-linked hole transport layers for high-efficiency perovskite tandem solar cells. *Sci. China Chem.* **64**, 2025–2034 (2021).
148. Al-Ashouri, A. *et al.* Conformal monolayer contacts with lossless interfaces for perovskite single junction and monolithic tandem solar cells. *Energy Environ. Sci.* **12**, 3356–3369 (2019).

149. Magomedov, A. *et al.* Self-Assembled Hole Transporting Monolayer for Highly Efficient Perovskite Solar Cells. *Adv. Energy Mater.* **8**, 1801892 (2018).
150. Bryant, D. *et al.* Light and oxygen induced degradation limits the operational stability of methylammonium lead triiodide perovskite solar cells. *Energy Environ. Sci.* **9**, 1655–1660 (2016).
151. Holzhey, P. *et al.* A chain is as strong as its weakest link – Stability study of MAPbI₃ under light and temperature. *Mater. Today* **29**, 10–19 (2019).
152. Di Girolamo, D. *et al.* Dual effect of humidity on cesium lead bromide: enhancement and degradation of perovskite films. *J. Mater. Chem. A* **7**, 12292–12302 (2019).
153. Howard, J. M. *et al.* Humidity-Induced Photoluminescence Hysteresis in Variable Cs/Br Ratio Hybrid Perovskites. *J. Phys. Chem. Lett.* **9**, 3463–3469 (2018).
154. Khenkin, M. V., M, A. K., Katz, E. A. & Visoly-Fisher, I. Bias-dependent degradation of various solar cells: lessons for stability of perovskite photovoltaics. *Energy Environ. Sci.* **12**, 550–558 (2019).
155. Lee, J.-W. & Park, N.-G. Chemical Approaches for Stabilizing Perovskite Solar Cells. *Adv. Energy Mater.* **10**, 1903249 (2020).
156. Conings, B. *et al.* Intrinsic Thermal Instability of Methylammonium Lead Trihalide Perovskite. *Adv. Energy Mater.* **5**, 1500477 (2015).
157. Zhao, Y. *et al.* Discovery of temperature-induced stability reversal in perovskites using high-throughput robotic learning. *Nat. Commun.* **12**, 2191 (2021).
158. Kim, M. *et al.* Methylammonium Chloride Induces Intermediate Phase Stabilization for Efficient Perovskite Solar Cells. *Joule* **3**, 2179–2192 (2019).
159. Ball, J. M. & Petrozza, A. Defects in perovskite-halides and their effects in solar cells. *Nat. Energy* **1**, 16149 (2016).
160. Fu, L. *et al.* Defect passivation strategies in perovskites for an enhanced photovoltaic performance. *Energy Environ. Sci.* **13**, 4017–4056 (2020).
161. Kosar, S. *et al.* Unraveling the varied nature and roles of defects in hybrid halide perovskites with time-resolved photoemission electron microscopy. *Energy Environ. Sci.* **14**, 6320–6328 (2021).

162. Hartono, N. T. P. *et al.* Stability follows efficiency based on the analysis of a large perovskite solar cells ageing dataset. *Nat. Commun.* **14**, 4869 (2023).
163. Khenkin, M. V. *et al.* Consensus statement for stability assessment and reporting for perovskite photovoltaics based on ISOS procedures. *Nat. Energy* **5**, 35–49 (2020).
164. Zhu, H. *et al.* Long-term operating stability in perovskite photovoltaics. *Nat. Rev. Mater.* 1–18 (2023) doi:10.1038/s41578-023-00582-w.
165. Gil-Escrig, L. *et al.* Efficient Wide-Bandgap Mixed-Cation and Mixed-Halide Perovskite Solar Cells by Vacuum Deposition. *ACS Energy Lett.* **6**, 827–836 (2021).
166. Guo, R. *et al.* Degradation mechanisms of perovskite solar cells under vacuum and one atmosphere of nitrogen. *Nat. Energy* **6**, 977–986 (2021).
167. Boyd, C. C., Cheacharoen, R., Leijtens, T. & McGehee, M. D. Understanding Degradation Mechanisms and Improving Stability of Perovskite Photovoltaics. *Chem. Rev.* **119**, 3418–3451 (2019).
168. Deretzis, I. *et al.* Stability and Degradation in Hybrid Perovskites: Is the Glass Half-Empty or Half-Full? *J. Phys. Chem. Lett.* **9**, 3000–3007 (2018).
169. Chi, W. & Banerjee, S. K. Achieving Resistance against Moisture and Oxygen for Perovskite Solar Cells with High Efficiency and Stability. *Chem. Mater.* **33**, 4269–4303 (2021).
170. McMeekin, D. P. *et al.* Intermediate-phase engineering via dimethylammonium cation additive for stable perovskite solar cells. *Nat. Mater.* **22**, 73–83 (2023).
171. Snaith, H. J. & Hacked, P. Enabling reliability assessments of pre-commercial perovskite photovoltaics with lessons learned from industrial standards. *Nat. Energy* **3**, 459–465 (2018).
172. Viperlab. *Viperlab* <https://www.viperlab.eu/>.
173. Jacobsson, T. J. *et al.* An open-access database and analysis tool for perovskite solar cells based on the FAIR data principles. *Nat. Energy* **7**, 107–115 (2022).
174. Myung, C. W. *et al.* Challenges, Opportunities, and Prospects in Metal Halide Perovskites from Theoretical and Machine Learning Perspectives. *Adv. Energy Mater.* **12**, 2202279 (2022).

175. Srivastava, M., Hering, A. R., An, Y., Correa-Baena, J.-P. & Leite, M. S. Machine Learning Enables Prediction of Halide Perovskites' Optical Behavior with >90% Accuracy. *ACS Energy Lett.* **8**, 1716–1722 (2023).
176. Liu, Y. *et al.* Exploring the Relationship of Microstructure and Conductivity in Metal Halide Perovskites via Active Learning-Driven Automated Scanning Probe Microscopy. *J. Phys. Chem. Lett.* **14**, 3352–3359 (2023).